ANALYSIS AND CORRELATION OF VOLCANIC ASH IN MARINE SEDIMENTS FROM THE PERU MARGIN, OCEAN DRILLING PROGRAM LEG 201: EXPLOSIVE VOLCANIC CYCLES OF THE NORTH-CENTRAL ANDES

A Thesis

by

SHIRLEY DAWN HART

Submitted to the Office of Graduate Studies of
Texas A&M University
in partial fulfillment of the requirements for the degree of

MASTER OF SCIENCE

December 2006

Major Subject: Geology

ANALYSIS AND CORRELATION OF VOLCANIC ASH IN MARINE SEDIMENTS FROM THE PERU MARGIN, OCEAN DRILLING PROGRAM LEG 201: EXPLOSIVE VOLCANIC CYCLES OF THE NORTH-CENTRAL ANDES

A Thesis

by

SHIRLEY DAWN HART

Submitted to the Office of Graduate Studies of
Texas A&M University
in partial fulfillment of the requirements for the degree of

MASTER OF SCIENCE

Approved by:

Co-Chairs of Committee,	D. Jay Miller
	Renald Guillemette
Committee Member,	Will Sager
Head of Department,	Richard Carlson

December 2006

Major Subject: Geology

ABSTRACT

Analysis and Correlation of Volcanic Ash in Marine Sediments from the Peru Margin, Ocean Drilling Program Leg 201: Explosive Volcanic Cycles of the North-Central Andes.

(December 2006)

Shirley Dawn Hart, B.S., Texas A&M University

Co-Chairs of Advisory Committee: Dr. D. Jay Miller
Dr. Renald Guillemette

A detailed investigation of cores from three Peru Margin sites drilled during Ocean Drilling Program (ODP) Leg 201 has been conducted to determine the occurrence of volcanic ash layers and ash accumulations within marine sediments along the Peru shelf. These sites were previously occupied during ODP Leg 112, which suffered from poor and/or disturbed recovery. Advancements in hydraulic piston coring realized since and employed during ODP Leg 201 resulted in better core recovery and less disturbance of sediment throughout the cored intervals. Since marine sediments potentially undergo less erosion and Leg 201 cores benefited from improved recovery, the tephrachronologic record from Leg 201 has yielded a more complete record of explosive activity for North-Central Andean volcanism than previous studies.

The improved recovery of Leg 201 cores has enabled the detailed examination of cores from the above sites needed to test the hypothesis that volcanic ash layers and accumulations are more abundant in the study region than previously reported. Due to

the low recovery of Leg 112 cores, Pouclet et al. (1993) document only six-ash layers, one ash pod, and eight ash-bearing layers (for a total of 14 cm of ash) from the three sites (Sites 684, 680, and 681) that were reoccupied during Leg 201 (Sites 1227, 1228, and 1229 respectively). This study reports a total of 332.0 cm of ash deposited into the study region which is approximately 24 times that previously reported.

Explosive eruption cycles for the Andean region have been deduced from the documentation of Leg 201 ash layers. Our record of volcanic cycles indicates that explosive activity was less intense during the Miocene, in which one ash layer (1.3 cm) was deposited, compared to that of the Pliocene and Pleistocene which experienced most of the explosive volcanic activity in which 52 ash layers (total thickness equal to 208.6 cm) and 14 ash layers (total thickness equal to 122.1 cm) were deposited respectively (Fig. 14). These data are consistent with the previous study of Pouclet et al. (1990); however these data indicate that explosive activity during the Pliocene and Pleistocene was more intense than previously reported.

ACKNOWLEDGMENTS

This research used samples and/or data provided by the Ocean Drilling Program (ODP). ODP is sponsored by the U.S. National Science Foundation (NSF) and participating countries under management of Joint Oceanographic Institutions (JOI), Inc. Funding for this research was provided by a grant awarded to D.J. Miller from the United States Science Support Program (USSSP) (http://www.usssp.iodp.org). I am grateful to Ray Guillemette for his time in running the microprobe and detailed discussions about microprobe analysis of volcanic glass samples.

TABLE OF CONTENTS

Page

LIST OF TABLES

LIST OF FIGURES

INTRODUCTION

Volcanic material commonly occurs in marine sediment as discrete ash-fall-out layers and/or disseminated ash accumulation within sediment deposits. Ash layers are useful indicators of explosive eruption cycles and can be used to calculate the approximate magnitude and duration of an eruption (Ledbetter and Sparks, 1979; Lackschewitz and Wallrabe-Adams, 1997; De Silva and Zielinski, 1998; Pattan, Shane, and Banakar, 1999; Shane, 2000). In order to determine the occurrence of volcanic ash layers and accumulations within marine sediment along the Peru shelf a detailed examination of cores from three Peru Margin sites (Fig. 1) drilled during ODP Leg 201 has been conducted.

Pouclet et al. (1990) determined the presence of volcanic ash layers and accumulations within Quaternary to late Eocene sediments in cores drilled along the Peru shelf during ODP Leg 112. They report a total of 30 ash layers, with the predominant amount of ash (8 layers: ~84 cm of ash deposited) occurring within the southern most site**;** ash layers were observed in the upper portion of the cored sections because the lower portion experienced poor recovery. Three (Sites 684, 680, and 681: Fig. 1) of the eight sites studied from Leg 112 were reoccupied during ODP Leg 201 (northern transect Site 1227 and southern transect Sites 1228 and 1229 respectively).

This thesis follows the style of Journal of Volcanology and Geothermal Research.

Pouclet et al. (1990) estimated the explosive activity in relation to time along the Andean Arc for the past 35 Ma through petrographic and chemical analysis coupled with the examination of the geographical and chronological distributions of the ash layers. Their data suggest that the record of explosive activity started in the late Eocene (~35 Ma) and continues into the Holocene with the bulk of activity occurring during the late Miocene (10 to 8 Ma) and Pliocene. However, the tephrachronologic record of Pouclet et al. (1990) may be incomplete due to the use of rotary coring techniques (extended core barrel [XCB] and rotary coring barrel [RCB]) of the lower portion of the cored sections, leading to the poor recovery (Table 1) of these deeper sections; hydraulic piston coring (APC) was used to drill the upper portion of the cored sections returning near-complete recovery and only slightly disturbed cores (Suess, von Huene et al., 1990).

Advancements in hydraulic piston coring employed during Leg 201 resulted in better core recovery and less disturbance of sediment throughout the entire cored sections (Table 1, for an explanation of drilling techniques see D'Hondt, Jorgensen, Miller et al., 2003) leading to a more complete sedimentological analysis of the region. Leg 201 Initial Reports (D'Hondt, Jorgensen, Miller et al., 2003) suggest abundant ash layers throughout core sections of Site 1228 that are not reported in corresponding sections of Site 680. For example, a 10 cm thick, pale blue ash layer in Core 201-1228A-6H-4 between 60 and 70 cm (Fig. 2) was observed during an initial reconnaissance of Leg 201 cores. Additionally, due to the low recovery of Leg 112 cores, Pouclet et al. (1990) document only six-ash layers, one ash pod, and eight ash-bearing layers from all three.

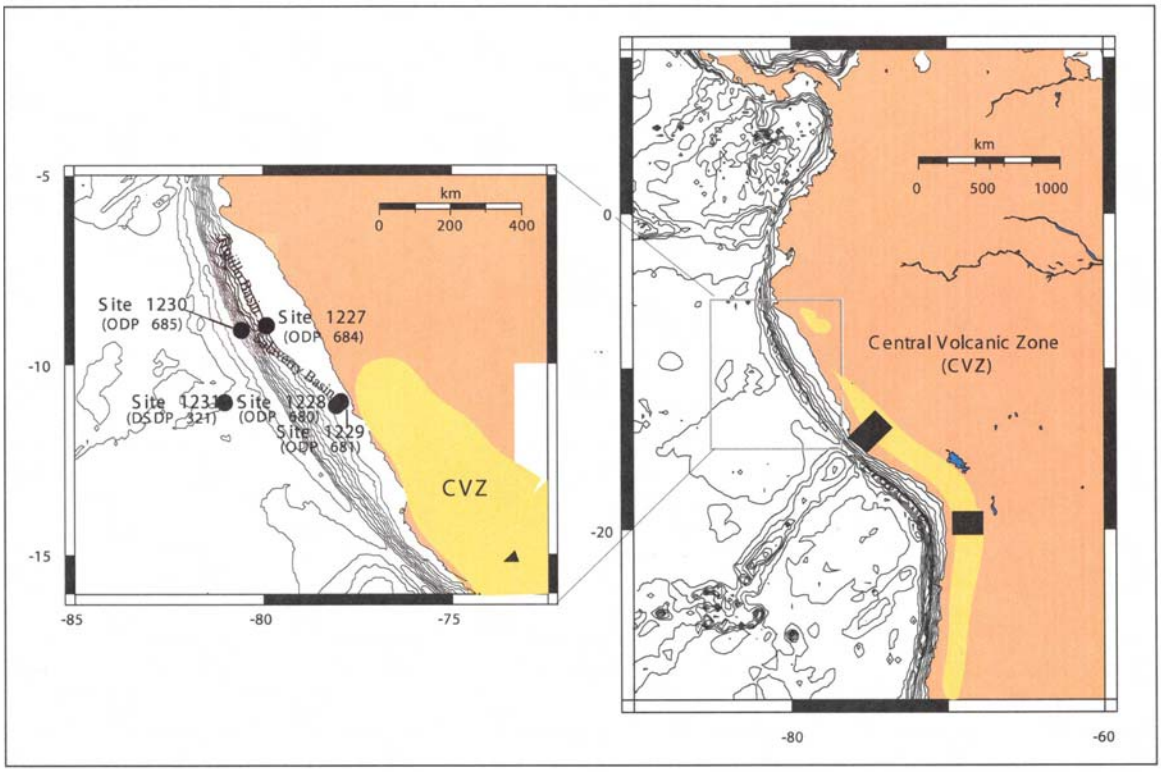

Figure 1: Site map. The location of the Central Volcanic Zone (CVZ) and land studies (black regions) are displayed and the inset (magnified to the left) displays Leg 201, Leg 112 (parentheses), and DSDP 34 site locations. The black triangle with the CVZ of the inset is the location of the northernmost active volcano (Huaynaputina) within the CVZ (de Silva and Francis, 1991). This site map is modified from Leg 201 Initial Reports (D'Hondt, Jorgensen, Miller et al., 2003).

Table 1
Leg 201 and Leg 112 recovery comparison. Comparison of core recovery between Leg 201 operations and previous occupation (Leg 112).

Leg	Site	APC depth (mbsf)	Recovery below previous APC depth
112	684	70	<3%
201	1227	150.51	66.50%
112	680	92	4%
201	1228	200.9	68%
112	681	111	22%
201	1229	194.4	44%

This table displays the percent recovery for the lower half of core for each Leg 201 site in this study, as well as each corresponding Leg 112 site. There was 100% recovery of the upper half of core.

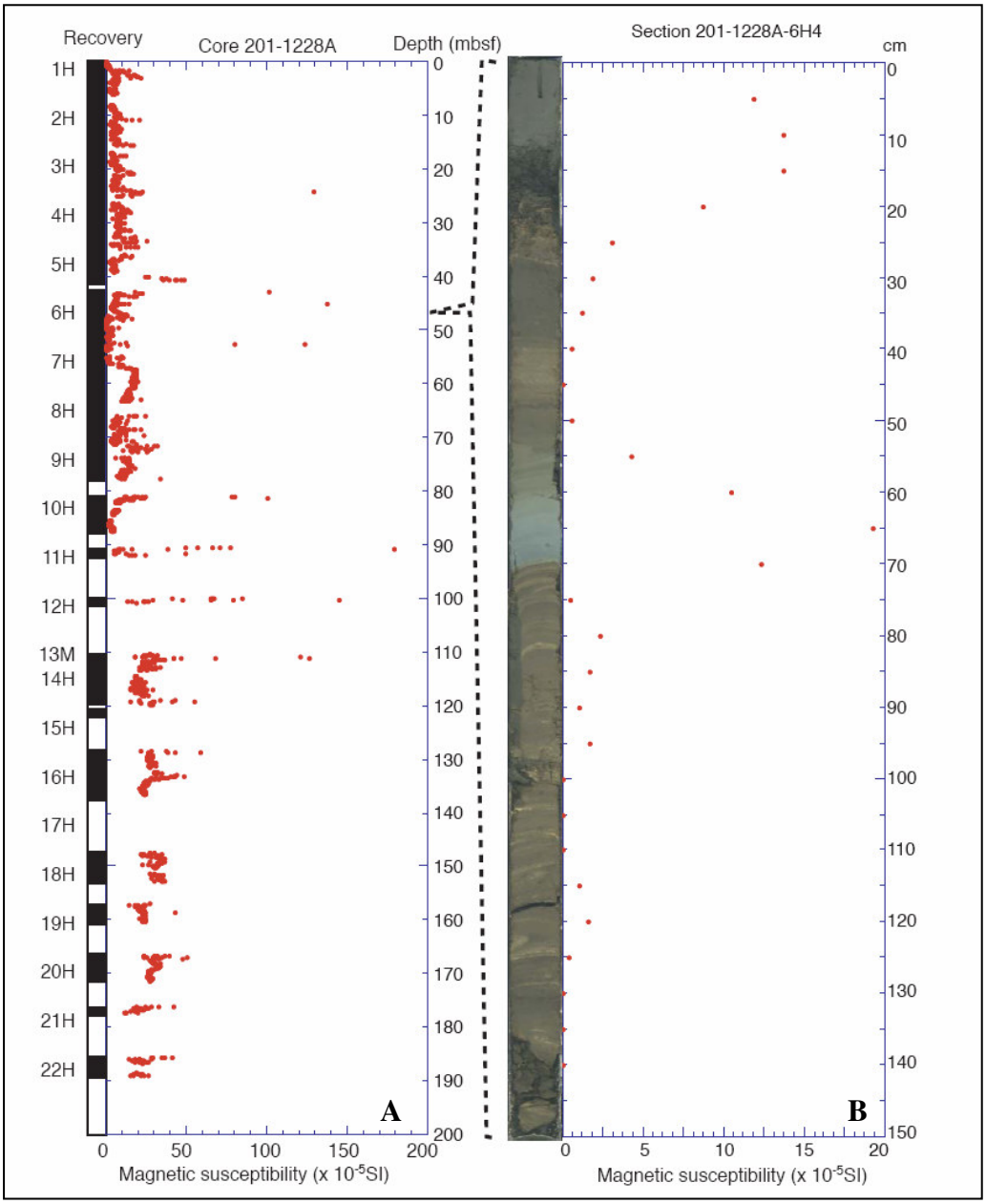

Figure 2: An example of the magnetic susceptibility record from Leg 201 Site 1228. A) Percent APC recovery is represented by the black region on the left side. The red dotted line represents magnetic susceptibility for both A & B. B) Digital core image from Section 201-1228A-6H-4 (the magnetic susceptibility is magnified in B, for this one section of core). The black stippled line shows the location of this section of core (B) within the entire hole (A). The numbers on the right of A are meters below the sea floor for the entire hole, whereas the numbers on the right of B are centimeters below the top of this section of core. Notice the magnetic susceptibility peaks in B line up with a probable ash layers. Figures A and B are from Leg 201 Initial Reports Volume (D'Hondt, Jorgensen, Miller et al., 2003).

previously occupied sites, whereas nine ash layers, in addition to the one reported above, are documented within the Initial Reports Volume for Site 1228 (Table 2, D'Hondt, Jorgensen, Miller et al., 2003).

A detailed description of cores and petrographic study of smear slides and grain mounts from Leg 201 sites have been carried out in order to determine the frequency of ash layers and accumulations within the marine sediment along the Peru Shelf. These data were also utilized to estimate the intensity of reworking and/or diagenesis of ash layers. Ash layers have been confirmed through whole rock geochemical analysis. This study has built upon the preliminary results from Leg 201 shipboard core descriptions, which describe numerous ash layers absent from the corresponding Leg 112 sites. This study has resulted in a more complete record of ash-bearing intervals (intervals are based on shipboard lithostratigraphic horizons and biostratigraphic dates) in the cores from the Peru Margin. These data complement land based tephrachronologic studies and have contributed to a better understanding of the episodicity of explosive volcanic activity in the Central Andes.

Table 2

Leg 201 volcanic ash locations reported in the Intial Reports Summary (D'Hondt, Jorgensen, Miller et al., 2003).

Cor-Sec	Cm	MBSF	Notes
Site 1227			
From Lilthostratigraphic Description			
7H-1			Not specifically stated: Throughout Unit IV (7H-1 to 18CC (core catcher).
From Core Description			
3H-1	116-118	16-26	Reworked volcanic glass layer
10H	throughout	81.6 - 91.1	Few volcanic accumulations
11H	Sporadic	91.1 - 100.6	Orange spots with plagioclase-bearing volcanic glass
12H	Org Spots	100.6 - 110.1	Rich in volcanic glass
13H-3		110.0 - 119.6	3 cm thich gray volcanic ash layer: yellow specks - volcanic glass
From Smear Slides			
3H-1	116	16.26	Plagioclase and silt-bearing volcanic ash (69% volcanic glass)
6H-3	135	47.95	Clay-bearing volcanic glass rich carb ooze (30% volcanic glass)
14H-2	70	121.8	Plagioclase-bearing volcanic ash (94% volcanic glass)
Site 1228			
From Lithostratigraphic Description			
1H-1		first 3 m	Few cm thick light gray volcanic ash layers
1H-2		first 3 m	Few cm thick light gray volcanic ash layers
3H		> 5m	3 ash layers, within 1H & 3H, varying in thickness from 4 and 6 cm show graded bedding and sharp basal contacts, indicating redistribution of terrigenous and volcanic material on the seafloor
4H-6			3 volcanic ash layers observed
6H-4	60		Parallel and cross laminations
6H-6	60		Parallel and cross laminations
From Core Descriptions			
1H-1	99	0.99	
1H-2	8	1.51	Light gray clay - silt rich layers (presumably of volcanic origin)
2H		4.9 - 14.4	Pale gray ash, layers containing few isotropic clasts, clay is abundant
3H		14.4 - 23.9	3 blue and gray volcanic ash layers (4 and 6 cm thick)
3h-7			One ash layer shows graded bedding and erosional base
4H-6		31.4	Contains 3 volcanic ash layers
6H		42.9 - 52.4	Pale blue gray ash layer: diatom bearing clay rich volcanic ash
10H			Orange spots rich in volcanic glass (disturbed cores)

Table 2 continued

Cor-Sec	Cm	MBSF	Notes
	From Smear Slides		
11H-2		91.4 - 93	Several sandy layers
1H-1	99	0.99	Diatom bearing volcanic glass rich silt
1H-2	132	2.73	Glauconite bearing quartz rich lithic silty sand
6H-4	70	48.1	Diatom bearing pyrite and clay rich diatom ooze (70% volcanic glass)
6H-6	62	51.02	Diatom and volcanic glass bearing dolomite (5% volcanic glass)
10H-3	29	84.1	Quartz and plagioclase and diatom bearing volcanic glass (84% volcanic glass)
	Site 1229		
	From Core Description		
5H		33.4 - 39.9	Gray layers are rich in quartz and contain feldspar and volcanic glass
11H		88.9 - 98.4	Few volcaniclastics throughout core
	From Smear Slide		
5H-4	66	38.56	Diatom-bearing volcanic glass-feldspar-quartz rich clay (20% volcanic glass)
11H-3	13	92.03	Volcanic glass bearing quartz - feldspar and silt rich clay (5% volcanic glass)
11H-5	73	95.63	Plagioclase - quartz rich volcanic glass (68% volcnic glass)

Cor-Sec = core and section number per hole. CM = centimeter location of ash within a given section of core.
MBSF = meters below the sea floor, depth of ash. Carb = carbonate.

GEOLOGIC SETTING

Subduction of the oceanic Nazca plate beneath the continental South American plate is responsible for the formation and volcanic processes of the Andes along the western edge of South America (Thorpe and Francis, 1979). Three linear zones of active volcanism are present along the Andean Cordillera (Fig. 3); northern volcanic zone (NVZ: 5°N – 2°S) located in Columbia and Ecuador, central volcanic zone (CVZ: 16°S – 28°S) primarily in south Peru and north Chile, but extending easterly into southwestern Bolivia and northwestern Argentina, and the southern volcanic zone (SVZ: 33°S-52°S) primarily in southern Chile and southern Argentina (Baker and Francis, 1978; Thorpe and Francis, 1979; de Silva and Francis, 1991).

The Altiplano of Bolivia and the Puna of northern Chile and Argentina dominate the CVZ (de Silva and Francis, 1991). These high plateaus, with elevations over 4000 m, separate a double mountain chain (the Western (Occidental) and Eastern (Oriental) Cordilleras, Fig. 3) in which the peaks are largely constructed of andesitic composite volcanoes (Baker and Francis, 1978; de Silva and Francis, 1991). Upper Cenozoic ignimbrite sheets are widespread along the western flanks of the Western Cordillera and the Altiplano and reach parts of the Eastern Cordillera (Fig. 3). These large ignimbrite sheets are also present within the Western Cordillera itself (Baker and Francis, 1978; Francis and Baker, 1978; Baker, 1981; Sparks et al, 1985; de Silva, 1989; de Silva and Francis, 1989). The Western Cordillera experienced the bulk of volcanic activity in this

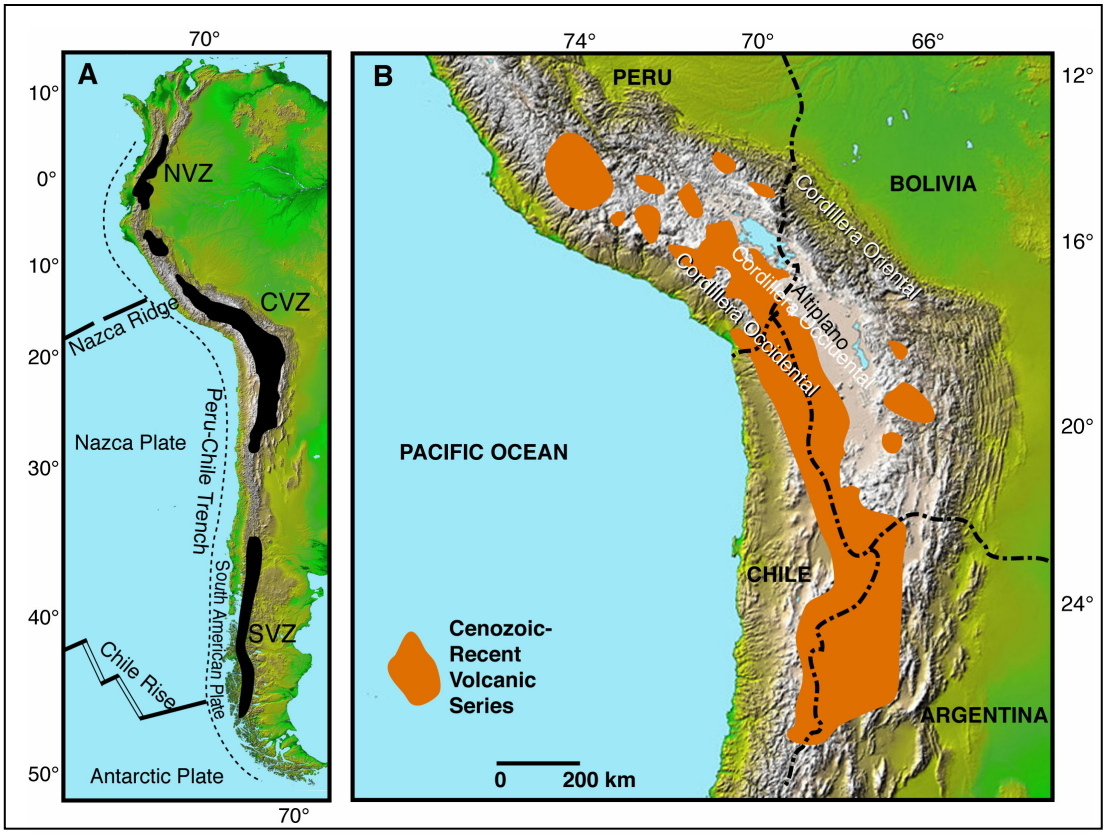

Figure 3: Prominent features of the Andes. The volcanic zones of the Andes northern volcanic zone (NVZ), central volcanic zone (CVZ) and the southern volcanic zone (SVZ)), the Nazca Plate and Ridge, Chile Rise, and the Peru-Chile Trench of this subduction zone are displayed in A. The Cordillera Occidental, Cordillera Oriental and the Altiplano of the Andes, as well as the Cenozoic to recent volcanic series (large scale ignimbrite sheets) for the region are shown in B. This figure has been modifiedfrom de Silva and Francis (1991), basemap is courtesy of NASA/JPL-Caltech.

Upper Cenozoic volcanic region, although a few unique events have occurred in the Eastern Cordillera in Bolivia (Baker and Francis, 1978; de Silva and Francis, 1991).

The large magnitude eruptions that deposited the extensive ignimbrite sheets along the western flanks of the Western Cordillera may also be responsible for the marine ash layers deposited in the study region due to the fact that "…an unknown, and possibly large, proportion of the erupted material would have been dispersed as fine-grained air-borne ash" (Baker and Francis, 1978). The ash layers discussed in this paper are believed to have been erupted from volcanic centers of the CVZ and were transported west northwestward into the study region by south–southeast winds and ocean currents (Fig. 4: Sparks et al, 1985; Garcia, 1994; Thouret et al., 1997; de Silva and Zielinski, 1998; Thouret et al., 2002). Therefore, the geologic history for only the CVZ is summarized below. However, these layers could have been erupted from volcanoes of the NVZ or SVZ of the Andes or other volcanically active regions of the world (e.g. Ledbetter (1985) studies volcanic ash deposited from volcanoes of Central America into the Pacific Ocean north of this study region (West of the region between Central and South America)). Detailed mineral and glass analysis would be required to deduce the precise provenance of each ash layer, which is beyond the scope of this study. The geochemical analysis of glass during this study has been conducted for a select sample set to demonstrate the probable Andean origin of the ash layers, not to distinguish the exact volcano from which the eruptions originated.

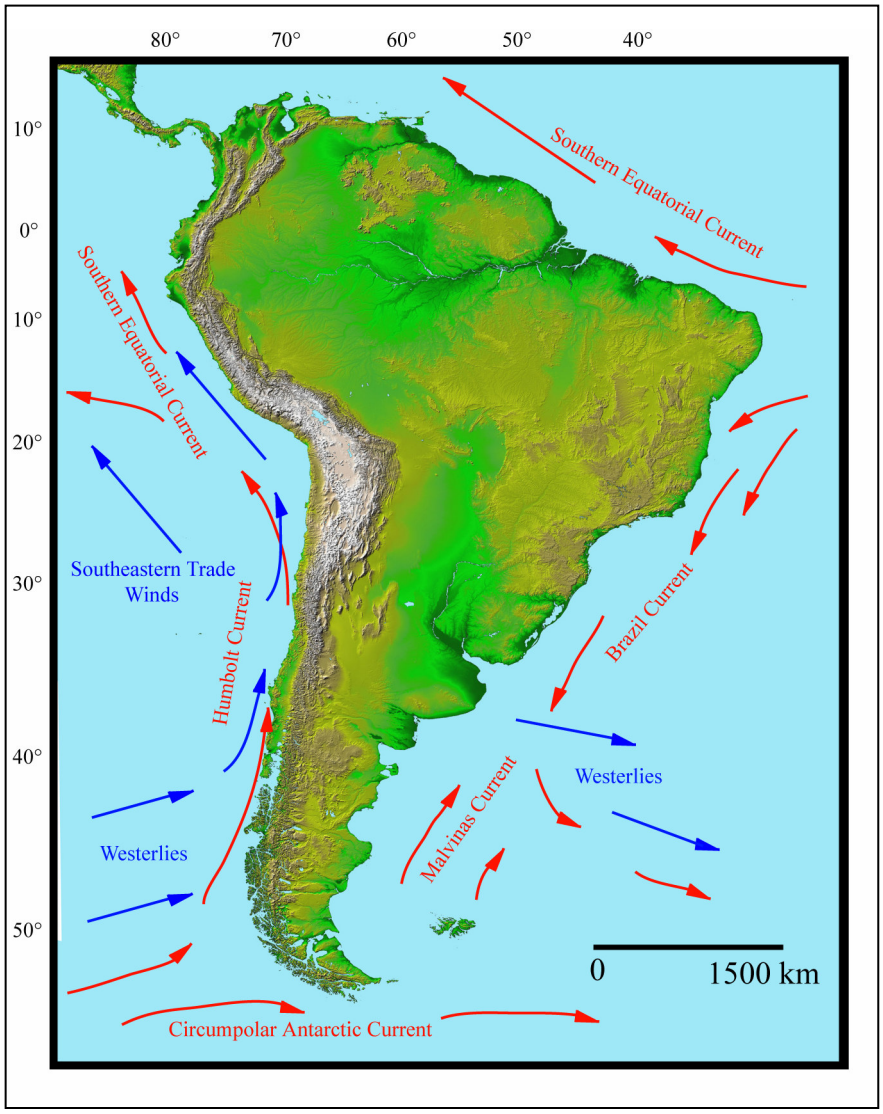

Figure 4: Prominent ocean and wind currents of South America. The flow paths of major ocean currents are shown in red and major wind currents are shown in blue. This map is modified from Garcia (1994), basemap is courtesy of NASA/JPL-Caltech.

PREVIOUS WORK

Marine Studies

Volcanic ash layers, pods (round to cylindrically shaped body of ash that are tapered at the ends and typically a few millimeters to centimeters in longest direction) and dispersed glass were observed within Quaternary to late Eocene sediment in cores drilled off Peru during Leg 112 of the Ocean Drilling Program (Pouclet et al, 1990). Pouclet, et al., (1990) collected 41 samples containing volcanic material from these cores. Of the 41 samples only four were from three of the sites reoccupied during Leg 201 (Sites 1227, 1228, and 1229). Of these four samples three were from ash layers (one ash layer within each of the Sites 684, 680 and 681) and one was from an ash pod from Site 680. In addition to these sampled ash layers and pod Pouclet et al., (1990) document through visual and petrographic analysis an ash pod from Site 684, eight ash-bearing beds (1-5 cm thick) from Site 680, and several occurrences of dispersed ashy material within several sections of core from all three sites. The ash within these sites have predominantly medium to high potassium (andesitic and shoshonitic), calc-alkalic, dacitic and rhyolitic compositions, with the exception of eight of the 41 samples analyzed that have andesitic compositions and no samples have low potassium (Pouclet et al., 1990). The origin of volcanic material was established through petrographic and chemical analysis and proved to be that of the Andean Volcanic Arc. These data coupled with the analysis of the geographical and chronological distributions allowed Pouclet, et al., (1990) to estimate the explosive activity in relation to time along the Andean Arc for the past 35 Ma. Their record suggests that explosive activity began in

the late Eocene (reports of sparse ash layers ~ 35 Ma) within the northern region (Sites 683, 684, and 685). Activity continued with two pulses during each of three Miocene series (lower, middle and upper Miocene). No ash layers were reported for the Pliocene; however two ash layers have been reported from the Pleistocene and Pleistocene-Holocene sections. The greatest explosive activity occurred during the upper Miocene for the northern region with eight ash layers depositing a total of approximately 28 cm of ash from 10 to 8 Ma (Pouclet et al., 1990).

Apparent explosive volcanic activity began during the lower Miocene in the southern region (Sites 679, 680, and 681) and continued through the Holocene. The Lower and middle Miocene series experienced one volcanic pulse each (16.5 – 15.5 Ma and 13.5 – 12.5 Ma respectively) and deposited approximately seven ash layers during each series; the total thickness of these ash layers for each pulse has been reported as approximately 17.5 cm (Pouclet et al., 1990). Apparent activity increased to two pulses within each series until the Pleistocene – Holocene in which only one pulse of perceived activity was recorded. The Pliocene marked a time of relatively intense activity with approximately seven ash layers depositing up to 60 cm of material between 5 - 4 Ma and 4 - 1.5 Ma. The record of volcanism is sparser through the Pleistocene section. Only two pulses (1.5 – 1 Ma and 1 – 0.5 Ma) of alleged activity occurred and deposited three ash layers with a cumulative thickness of approximately 3.5 cm of ash. Apparent activity picked up once again during the Pleistocene – Holocene with one volcanic pulse from 0.5 Ma producing five ash layers, which deposited approximately 20 cm of ash (Pouclet et al., 1990).

Vigorous volcanic activity is recorded in the sediments from the southern most sites (686 and 687) as occurring from the Pliocene through the Pleistocene – Holocene. There was one large pulse of apparent activity during the Pliocene (2 – 1.65 Ma) that deposited three ash layers with a cumulative thickness of approximately 14 cm. This activity continued into the Pleistocene with two more large pulses (1.65 – 1 Ma and 1 – 0.5 Ma) depositing six ash layers with a cumulative thickness of 32 cm. The Pleistocene – Holocene is marked with one more large pulse (0.5 – 0 Ma) of volcanism, depositing five ash layers with a cumulative thickness of 22.5 cm (Pouclet et al., 1990). These southern most sites are evidence of a time of intense volcanism within the CVZ with a cumulative thickness of 68.5 cm of volcanic ash deposited within both sites.

This record of apparent explosive volcanic activity reported by Pouclet et al., (1990) depicts variations in eruptions cycles on land evidenced by the variation in the number of ash layers deposited within cores from the northern and southern sites of Leg 112. They report ash deposits indicative of intense volcanic episodes during the Pliocene – Quaternary time periods at the southern sites that do not occur at the northern sites. For example they report up to 74 cm of tephra per 0.5 Ma in the upper Pliocene within the southern and southern most sites and no tephra deposits are recorded at all within the Pliocene sediments of the northern sites. In addition they report a sizeable decrease in explosive activity throughout the Pleistocene and Pleistocene – Holocene (~ 2 cm of ash deposited total for both times) for the northern sites, whereas these times yield a large amount of tephra (~93 cm total for the entire time range) within the southern and southern most sites indicating an increase of explosive activity for this region. Pouclet et

al., (1990) attribute this variation to the seismic gap of the northern Peruvian Andes located between 3° – 16° S latitude.

The summary of volcanic cycles depicted within the marine cores above does not include Site 1231, which is a reoccupation of DSDP Leg 34 Site 321; the western most site occupied (Fig. 1). Donnelly (1976) estimated accretion rates of volcanic material along the Peru margin over the past 10 Ma from spot samples containing dispersed volcanic constituents from this site. He reports that the late Miocene to present sediments record moderate amounts of volcanic activity during these time periods. The age and chronology of volcanic debris, for both studies, was determined using estimated sedimentation rates established from biostratigraphy (Suess, von Huene et al., 1990; Yeats, Hart et al., 1976).

Land Studies

The CVZ of the Central Andes is one of the largest volcanically active regions of the world (Francis and de Silva, 1989; de Silva and Francis, 1991). The principal magma source for the andesitic volcanoes of the CVZ is believed to be derived from the partial melting of an asthenospheric wedge between the overriding continental South American plate and the descending oceanic Nazca plate (Fig. 3, Baker and Francis, 1978; Hanus and Vanek, 1978; Thorpe and Francis, 1979; de Silva and Francis, 1991). This magma source produced Late Cretaceous (Aptian stage (114 – 108 Ma)) through Quaternary subaerial volcanic sequences of andesite, basalt andesite and rhyolite to rhyodacite lavas, tuffs and volcaniclastics that were deposited throughout the Central Andes (Noble et al.,

1974; Baker and Francis, 1978; Francis and Baker, 1978; Tosdal et al., 1981; Baker, 1981; Lahesen, 1982; Hall and Calle, 1982; Sparks et al., 1985; de Silva and Francis, 1989; de Silva, 1989; Lindsay et al., 2001). Detailed studies of these deposits have been conducted by combining field data and Landsat (Thematic Mapper) images. These studies have reported ash flow tuff and ignimbrite deposits covering large areas of the CVZ and having volumes of several hundred cubic kilometers (Baker and Francis, 1978; de Silva and Francis, 1989; Lindsay et al., 2001). Ash fall covering an area of 300,000 km^2 and having an approximate volume of 8.8 km^3 (combined air fall ash and pyroclastic tephra has a volume of 19.2 km^3) has been documented for one historically large eruption, that of Huaynaputina located at 16°35' S, 70°52' W in southern Peru (the northern most portion of the CVZ, Fig. 1). This eruption has been described as the largest historic eruption of the Andes with ash fall deposits 5 cm at a distance of 200 km away from the source (de Silva and Zielinski, 1998; Adams et al., 2001).

Intense volcanic activity during the Middle to late Miocene and into the Pliocene followed the re-inception of volcanic activity along the CVZ during the early Miocene (Noble et al., 1974; Baker and Francis, 1978; Tosdal et al., 1981; Lahesen, 1982). A thick layer of tuff and lava from this active zone was believed to blanket a large part of the Central Andes during this time period (Noble et al., 1974). Baker and Francis (1978), as well as other authors (Francis and Baker, 1978; Tosdal et al., 1981; Baker, 1981; Sparks et al., 1985; de Silva, 1989; de Silva and Francis, 1989), have documented the existence of large dacitic and rhyodacitic ignimbrites, some covering areas in excess of 2300 km^2 within the Central Andes (Francis and Baker, 1978). Although these

formations may cover large areas of the Andes, lavas (typically andesitic) still dominated the region volumetrically into the Pliocene (Baker and Francis, 1978); however, there are local areas where ignimbrites dominate the volcaniclastics stratigraphy in volume and area (de Silva, 1989). The general agreement among authors is that these extensive ignimbrite eruptions began during the late Miocene and continued into the Pliocene, which is concurrent with the eruption periods from the marine studies of Pouclet et al. (1990). An abundant amount of small and large strato-volcanoes formed along the Cordillera Occidental of southern Peru and northern Chile in the early Pliocene with the progression of voluminous calc-alkaline, intermediate lava flows (Tosdal et al., 1981; Lahesen, 1982). These andesitic flows succeeded the large volume ignimbrite eruptions from the upper Pliocene through the Quaternary (Baker and Francis, 1978; Tosdal et al., 1981). A number of large stratovolcanoes that initially developed during the Pleistocene accommodated Holocene volcanism within the CVZ (Tosdal et al., 1981). Baker and Francis (1978) reveal regional variations in volcanic episodicity within the northern (19°30'S to 21° S) and southern (21°to 22°30'S) parts of the central portion (19°30'S to 22°30'S) of the CVZ. These variations occur from the lower Miocene through the Holocene and are presented first for the total volume of volcanic material erupted (lava flows plus ignimbrite deposits) and secondly for the ignimbrite deposits alone and are as follows: in the northern portion of their study area two periods of peak activity occurred from 12 to 9 Ma (middle Miocene) and 6 to 3 Ma (late Miocene - early Pliocene), whereas in the southern region of their study area the largest volume of material was erupted from 6 to 0 Ma (late Miocene to Holocene). The largest volume of ignimbrites

was deposited during the early Miocene, 150 km^3 (22-18 Ma) and 500 km^3 (18-15 Ma) totaling 650 km^3 in the northern study region. In addition Baker and Francis (1978) record two more deposits of 150 km^3 each during the late Miocene 9-6 Ma, and late Miocene-early Pliocene 6-3 Ma, one deposit of 75 km^3 (early Pliocene – Holocene 3-0 Ma), and one deposit of 50 km^3 (middle Miocene 15-12 Ma). In their southern region Baker and Francis (1978) report ignimbrite eruptions beginning during the middle Miocene (12-9 Ma) with the largest deposits occurring within the late Miocene – early Pliocene (6-3 Ma) depositing 500 km^3 of material. In addition two deposits of 250 km^3 have been recorded during the middle Miocene (12-9 Ma) and early Pliocene to Holocene (3-0 Ma) and one deposit of 200 km^3 was deposited during the late Miocene (9-6 Ma) (Baker and Francis, 1978). These large ignimbrite deposits are of the most significance when correlating marine ash (air fall) layers with land studies since they give evidence for the occurrence of airborne ash (Baker and Francis, 1978) and of large plinian style eruptions, which can produce a significant amount of air-fall ash (Fisher and Schmincke, 1984). Tosdal et al., (1981) have performed a geochronology of southern Peru (the northern most region of the CVZ) pertaining to late Cenozoic (Miocene – Holocene) volcanic rocks. Their record indicates five separate rhyodacite ignimbrite formations in which eruptive episodes began in the late Oligocene and continued through the Miocene and into the earliest Pliocene. Andesite and dacite lava flows predominated throughout the Pliocene (Tosdal et al., 1981). Tosdal et al.'s, (1981) record of eruption cycles best matches that of Baker and Francis's (1978) northern region with most ignimbrites being deposited during the late Miocene.

Pouclet et al., (1990) also report variations within Andean eruption cycles recorded within the northern and southern sites of Leg 112 cores. They report a similar pattern of cyclicity as above with the only major difference being the lack of volcanic deposits during the Pliocene within cores from the northern sites. This difference could be attributed to the fact that there is a large distance between the land study regions and the northern sites of Leg 112 (approximately 1000 km and greater: Fig. 1) and the Pliocene eruptions may not have been as large as earlier eruptions, therefore ash from these eruptions have made it to the southern sites but not the northern ones.

METHODS

Five holes were drilled for ODP Leg 201 Sites 1227, 1228 and 1229 (D'Hondt, Jorgensen, Miller et al., 2003). Cores from the initial hole (A) of each site were chosen for examination during this study since this hole obtained the deepest penetration (150.51 mbsf, 200.9 mbsf, and 194.4 mbsf respectively), the greatest average recovery of sediment (Table 1) and 100% recovery of the upper half of the hole at each site (D'Hondt, Jorgensen, Miller et al., 2003).

The frequency and curated depths of ash layers and accumulations have been documented through the relogging of cores at the Integrated Ocean Drilling Program (IODP) Gulf Coast Repository at Texas A&M University. The occurrence of ash layers was determined through detailed visual core and smear slide analysis (a toothpick sample smeared onto a slide, dried on a hotplate and a cover slide is glued on with ultraviolet light setting epoxy) and their ages have been inferred from the biostratigraphy of corresponding Leg 112 sites. The attempt to use magnetic susceptibility to verify the occurrence of ash layers less than one half millimeter thick, which are too thin to sample and verify through geochemistry, failed due to the relatively low content (<0.5 % petrologically) or lack of magnetic minerals (predominantly magnetite) within Leg 201 ash layers; prominent peaks occurred within beds containing high amounts of biologic material.

Ash layers were initially distinguished upon visual examination based on color (blue-gray, gray, tan-gray-black, and cream) and lithology (coarser grained than surrounding ooze). Petrographic analyses of smear slides were conducted in order to confirm and categorize volcanic ash material. Ash layers and accumulations were categorized based on the percent biogenic material or diagenesis present. Type 1 ash layers were defined as layers that contain 1) ≤ 5 % biogenic component and 2) ≤ 1-2% rounded grains. Additionally, all Type 1 ash layers were also required to possess either 1) a large percent (≥ 10%) of glass/pumice or 2) lesser glass/pumice (1-2%) and at least 0.5 – 1 % amphibole or biotite. Ash layers that met these criteria were sampled for whole rock geochemical analysis for confirmation. These layers are interpreted to be undisturbed, primary depositional horizons. Type 2 ash layers contain biogenic or dolomite content >20% but <60%, Type 3 ash layers contain biogenic material >60%, and Type 4 ash layers contain >60% dolomite. Type 4 ash layers would be considered Type 1 in the absence of diagenesis.

Sixty-eight bulk aliquot samples from distinct ash layers were sent to Acme Analytical Laboratory for ion coupled plasma (ICP) analysis for major, trace, and rare earth elements (REE) (whole rock compositions were determined through ICP-AES (atomic emission spectroscopy) and ICP-MS (mass spectroscopy) analysis). Precision and reproducibility of the results were evaluated, respectively, through the use of USGS standard reference materials submitted for analysis as unknowns and duplicates. A second portion of the sampled ash layers was passed through a 63-µm sieve to remove

clay-sized particles. Grain mounts were prepared with grains ≥ 63 μm. Major and minor elements have been determined for glasses from each grain mount using the Texas A&M Cameca SX 50 electron microprobe. These analyses were run with an accelerating voltage of 15 kV, a sample current of 10 nA, a beam diameter of 10 to 12 μm, and a count time of 20 to 40 s. Three glass standards (one Yellowstone glass, one tektite, and three basaltic glasses) were used for calibration and standard checks were run once on all five glasses and three times on the Yellowstone glass to test for precision and reproducibility of the analysis. These data were used to confirm the origin of Leg 201 ash content and to classify, and correlate ash layers.

Total alkali versus silica (TAS) and K_2O vs. SiO_2 diagrams have been utilized to classify the chemical composition of these ash layers. Major oxide versus silica oxide and rare earth element (REE) plots were created and compared with bivariant and REE plots from land studies in order to deduce the primary volcanological province from which the ash was erupted.

The correlation of ash layers between sites has been attempted through the use of stratigraphic position, lithology, and geochemistry of layers. A detailed stratigraphic section has been created to display the distribution and correlations of Primary ash layers for each site. Hiatuses are correlated between sites and are used as markers for ash layer associations. Major element oxides versus silica and REE plots have been created from

whole rock geochemistry in order to distinguish geochemical correlations that may exist between sites.

RESULTS

Leg 201 sediments consist of inter-bedded diatom, foram, and nanofossil oozes (Suess, von Huene et al., 1990). These beds are olive green, dark green, brown or black with yellow-tan laminae and range in grain size from clay to sand. Volcanic ash layers, laminae and/or accumulations are also present within cores from all three sites (Table 3, for location of ash layers within cores see appendix A). Volcanogenic deposits are abundant within Sites 1228 and 1229 and are dispersed throughout most of the cores at these sites. These deposits are scarce at Site 1227 and are restricted to the upper and lower three cores (Cores 1227A-(1H-3H, 11H-13H) respectively) at this site.

Some ash layers were easy to recognize during the visual examination of cores due to their strong color contrast to biogenic sediments (gray, tan-gray and black, and cream) while others were darker in color (black or brown) and resemble biogenic beds. The ash layers in this study tend to be coarser grained than the biogenic material above and below them, signifying a change in lithology. This change in lithology aided in the distinction between darker colored ash layers and biogenic sediments. Although color and grain size are useful indicators of possible ash occurrences during the visual examination of cores, some layers that visually resembled a typical ash layer (bluish gray colored very fine silt to silt) proved to be composed largely of biological sediment after smear slide evaluations. For example the 10 cm bed in Core 1228A 6H-4, 60-70 cm discussed previously proved to be composed of ~70-85% biogenic material.

Table 3
Leg 201 ash layer description.

Sample #	LayerThkns (cm)	Depth MBSF	Lithology (approximate percent) Biogen	Gls-Pum^{+1}	Rndns (Qz)	Description, Structure and Contact
Site 1227 Miocene						
*27A-1	1.3	115.07	na	(98-99) - na	na	buff silt to very fine sand, top gradational, bottom may be erosional
Site 1228 Pliocene						
28A-5	0.5	64.24	1	1 - 3	1-2	light gray fine silt-clay, 3-5% dolo, thins in center, poorly sorted, top gradational-bottom broke
*28A-6	3.0	66.04	1-2	1 - 30		light silt, ~5% dolo, clay pod in base, moderate-well sorted, top-convex to right
*28A-10	2.2	72.09	1	50 - na	na	cream clay, ~45% GM, few dark coarse xtls, convex to left contacts, one flaser mark
28A-11	1.0	72.12	<=1	(0.5-2) - 75	1-2	brown silt, ~1%dolo, pumice-round, bottom-gradational both slightly wavy
*28A-12	2.5	72.15	1-2	1.5 - 5	1-2	light gray silt, ~4%dolo, ~20% coated grains, top-gradational wavy, bottom-slightly inclined
28A-13	1.5	72.22	1-3	1.5 - 20	3-5	brown silt (angular), ~3-5% round pumice, top sharp to gradational, bottom gradational-inclined
*28A-14	4.6	72.37	na	(1-2) - (3-5)	na	gray-tan silt, ~80% glass coated grains+2, normally graded, top gradational
*28A-16	2.6	72.61	1	1.5 - (15-30)	1-2	gray-tan silt, ~5% round pumice, ~2-3%dolo, normal grading, <=60% pumice & ~15% dolo in bottom half
*28A-19	25.5	91.73	na	1 - (30-40)	<0.5	gray-tan-black coarse silt-sand, ~1-2% round pumice, thins-rt~1.8 cm's, bottom slightly inclined
*28A-20	2.1	91.90	na	80 -(3-5)	1-2	blck-brwn clay, ~3-5% round pumice, finely laminated top convex, bottom slight incline, both gradational
28A-21	2.7	91.93	na	75 - (1-3)	1-2	tan-cream fine silt, ~2% round pumice & 55% groundmass, finely laminated, gradational-slilghtly-inclined
*28A-22	1.6	91.95	1-3	30 - 10	1	gray-brown-gray- silt with ~20% groundmass, normal grading, slightly inclined, top-gradational,
*28A-23	1.6	91.99	<1	70 - 10	na	cream silt, poor-mod sorted, sharp-top slight-ripple, bottom planar: possible correlation w/1227A 13H-2
*28A-25	3.6	111.98	3	(1-2) - (20-30)	<1-1	tan-brown-gray coarse silt; distinctly more coarse than layers above and below
28A-26**	1.0	113.06	10	<1 - 20	1	gray-tan-brown silt to sand, ~1% round pumice, thins slightly (1-2mm), gradational, bottom slightly scoured
28A-27	0.9	123.19	3-5	na - 20	1-2	orange silt (gray ~ 2 mm below surface); ~30% groundmass, bottom slightly wavy
28A-29**	5.0	113.34	5-10	0.5 - 60	na	tanish-gray silt; ~3-5% ooids; thinly laminated; top planar, bottom end of core
*28A-30	6.2	116.93	<=5	(1-3) - (30-50)	1	gray-tan silt; ~20% coated; top partly scoured (filled with laminations), bottom slight break

Table 3 continued

Sample #	Layer Thkns (cm)	MBSF	Lithology (approximate percent) Biogen	Gls-Pum^{+1}	Rndns (Qz)	Description
28A-31	3.5	117.37	1-2	1 - 80	1	ceam-lt gray silt, bottom cm tan (10-15% biogenic); top broken wavy, bottom slightly wavy
*28A-32	4.2	117.57	1-3	1 - (30-40)	<1	tan-gray (orangish) silt, ~1 mm laminae at the top
28A-33	1.0	117.72	1-3	0.5 - 60	na	tan-cream silt, thins to the left, top sharp wavy, bottom planar - broke
*28A-34**	5.7	118.07	5-10	1 - 80	1-2	brown silt, ~50% biogenic in bottom cm, top concave, bottom slilghtly wavy
28A-35**	3.0	118.14	-5 -> 5-1(	(1 - 15) - >80	1	gray-tan silt, sharp, top slightly wavy, bottom concave, pumice&biogenic increase bottom cm
*28A-37	6.5	128.77	2-3	(2-3) - (15-25)	<=0.5	gray silt, ~20% groundmass (~5% at bottom), top slightly rippled
*28A-38	4.0	128.84	1	2.5 - 20	<1	gray silt, planar, bottom gradational
*28A-39	4.0	129.00	<=1	1.5 - (20-30)	<1	gray silt, gradational planar contacts
*28A-40	2.5	129.05	<=3	2.5 - 50	<=1	gray silt, top wavy, bottom planar
28A-41	4.0	129.32	1-2	1.5 - 60	<1	gray silt, top planar, bottom wavy
28A-42	1.2	129.51	1-2	0.5 - 70	<1	gray silt, light tan-light cream laminae
28A-43	3.5	129.54	1-2	2.5 - 70	<1	gray-light cream interlaminae, finely laminated, top and bottom convex up
*28A-45	4.5	129.59	1-2	2 - 70	<1	gray silt, few discontinuous laminae
28A-46	1.0	129.72	1-2	2 - 20	<=1	gray silt, ~70% coated grains, top planar, bottom end of core
*28A-47	3.5	130.03	1-2	(1-1.5) - 80	na	gray silt, tan-finely laminated, gradational convex up to the right
*28A-49	6.5	130.18	1	2.5 - (60-70)	<-0.5	gray silt, one tan lamination (~1mm) in center
*28A-50	5.5	131.09	1-2	2 - (60-70)	<=0.5	gray silt, tan finely laminated, ~3-5% ooids
*28A-54	2.5	132.35	1	0.5 - (940-50)	na	tan silt, one brown lamination, ~5% ooids, top sharp, bottom gradational slightly wavy
*28A-56	3.5	132.51	1-2	1 - 60	1-2	tan finely laminated silt, bottom gradational, both slightly wavy
*28A-57	3.5	132.58	1-2	1 - 15	<1	tan silt, ~15% round pumice, top convex up bottom rippled
*28A-59	13.5	133.17	na	1 - 30	1	gray silt, ~15% round pumice, top gradational, both planar
*28A-60**	2.0	133.31	20	5 - 30	<=1	gray-tan finely laminated silt, biogenic-ostracods
*28A-64	8.5	147.88	1-3	2 - 60	<=0.5	gray silt, gray-tan up to 51 cm (gradational), ~1% round pumice, ~5-10% groundmass
*28A-65	5.0	148.02	1-2	2 - (70-80)	<=0.5	gray silt, ~2-3%round pumice, top inclined, bottom planar
*28A-67	3.7	148.96	1-2	2 - 70	<=0.5	gray-tan finely laminated silt, ~1% round pumice, top convex at right side
*28A-70	7.0	149.41	3	2 - 70	<0.5	tan-brown silt, top half slightly laminated (54.5-gradational) lower half laminated, ~1% round pumice
*28A-71	3.2	149.70	1-3	2 - 70	<0.5	tan-brown finely laminated silt, ~1% round pumice, top wavy, bottom convex to right

Table 3 continued

Sample #	LayerThkns (cm)	MBSF	Lithology (approximate percent) Biogen	Gls-Pum^{+1}	Rndns (Qz)	Description
*28A-73	2.0	149.78	1-2	2 - 70	<0.5	cream silt, ~1% round pumice, vesicular glass present, convex bed
*28A-75	3.0	150.02	1-2	2 - 90	<0.5	tan silt, ~3-5% round pumice, top slightly convex to right, bottom end of core
*28A-76	1.5	151.36	1-3	(1-1.5) - 80	1-2	gray-tan silt;,~1-2% round pumice
*28A-77	3.0	151.95	1-2	2 - 70	<0.5	tan-gray silt, ~1% round pumice, some bioturbation, bottom gradational planar
*28A-80	4.0	152.28	1-2	2 - 70	<0.5	tan silt, ~1% round pumice, top wavy, bottom planar
*28A-81	6.0	152.35	1-3	2 - 70	<0.5	tan and cream silt, ~1% round pumice, brown pod at top
*28A-82	4.5	152.74	1-2	2 - 70	<0.5	tan silt, ~1-2% round pumice, top slightly wavy sharp bottom sharp planar and slightly bioturbated
Site 1229 Pleistocene						
29A-a	0.3	2.50	<= 3	2 - 3	na	gray silty xtl-pumice-hash, discontinous, inclined lamina, top-gradational
*29A-1**	0.5	17.90	10-15	75 - na	na	gray-white clay lamina, planar, top - gradational
*29A-2	3.0	40.66	1 - 2	3 - na	1	white-cream silt, fines upward, slightly inclined and gradational-contacts
*29A-3**	1.3	43.09	5-10	2 - 5	na	gray-tan clay, slightly inclined, thins to one end
*29A-4	1.8	69.97	0.5	< 1 - 10	2-3	gray silt, ~10-25% dolo, fines upward, inclined, top-gradational
*29A-4	0.2	69.99	<= 5	3 - na	1-2	cream, xtl hash, very fine silt lamina, inclined
*29A-6	7.0	85.77	3-5	(1-3) - na	2-3	gray clay, ~3-5%dolo, fines upward
29A-b**	4.5	91.92	5-10	<= 1	10-15	gray-tan silt, ~3-5%dolo, fines upward
*29A-7	2.7	91.97	1-3	(1-2) - 10	1-2	gray-tan silt, ~1-3% dolo, coated grains account for a majority of round grains
29A-c	TL	92.00	1-3	(0.5-1) - na	<1	light colored discontinous silt lamina, ~20-30% coated grains
29A-d**	0.3	92.29	5-10	(1-2) - (5)	na	light colored discontinous silt lamina, ~3-5%dolo, bottom-gradational
29A-e**	1.0	92.80	10-15	(2-3) - na	na	light gray silt between gray clay beds, dolo ~5%, 5-10% opaques, normal grading
29A-f**	0.2	118.28	1-3	<1 - na	na	cream silt, ~10-15%dolo, pinches out
29A-h**	TL	123.29	5-10	<1 - (10-15)	na	gray-tan-brown silty sand, slightly inclined
*29A-8**	6.0	123.90	3-5	(2-3) - --	<= 1	cream-gray-black silt, fines upward, ~10-20%dolo
*29A-9	3.0	155.40	3-5	(1-2) - (15-20)	na	gray-tan silt, ~1-2%dolo
29A-j**	49.0	155.65	5-10	(1-2) - (50-60)	na	gray-tan silt, 2 tan laminae-biogenic, fine-planar-laminae, bottom-inclined
*29A-11	0.5	158.07	1-3	(1-2) - na	na	gray-white-orange sandy silt lamina

Table 3 continued

Sample #	Layer Thkns (cm)	MBSF	Lithology (approximate percent) Biogen	Gls-Pum^{+1}	Rndns (Qz)	Description
*29A-12	0.2	158.07	3-5	1 - 10	na	gray-white sandy silt lamina, bottom - gradational
*29A-13	9.6	156.17	3-5	(1-2) - (10-15)	na	gray-tan silt, ~1-2%dolo, top-gradational
*29A-14**	8.0	159.88	5-10	(1-2) - na	na	gray-white poorly sorted feldspar-quartz silty sand with in reworked bed, planar
*29A-16**	7.5	159.55	10-15	1 - (5-10)	na	gray-tan sandy silt, bottom- break
29A-17	4.5	122.08	<=10	(1-3) - na	na	gray-cream clay, GM is first order gray & white, discontinous laminae and pod
29A-18**	11.0	123.73	3-5	to fine to tell	na	cream clay, ~5-10-15% dolo, xtl rich pods of dolo, slightly concave contacts

Sample number is distinguished as follows: 27A-1 is equal to the first sample from core 1227A (these nun numbers match those from whole rock geochemistry). See Appendix A for a list of sample locations within each core.
Samples with letters (29A-a) are ash layers that were not sampled for bulk geochemistry.
Unless otherwise specified contacts between layers are planar and sharp.
Layer Thkns = layer thickness, Biogen = biogenic (component), Gls-Pum = Glass - Pumice %
Rndns = % roundness, Qz = quartz.
* = Whole rock geochemistry has been acquired for these layers (Table 6).
** = Layer is borderline (10-15% biogenic material or dolomite).
na = not applicable; the feature was not observed.

Ash Layer Description

Ash layer contacts are primarily sharp, with some contacts being gradational. Three layers in Site 1228 and five layers in Site 1229 are normally graded, the rest are either homogenous or slightly graded (1-2% more coarser grains present in the lower portion of the layer than at the top).

Type 1 ash layers present in each site are described in Table 3. Figure 5 displays a representative ash layer sample from each site. Type 2 through Type 4 ash occurrences are recorded in Table 4, and all ash content is summarized below. Because I elected to use the arbitrary boundary of 10-15% nonprimary components to define the limit of Type 1 layers, I adopt the term borderline ash accumulations for those samples that are within the error of visual estimate of content (±2%-3%).

Site 1227 Ash Layers

Site 1227 is located on the upper slope of the southeastern edge of the Trujillo Basin (Fig. 1) at a water depth of 427.5 m (D'Hondt, Jorgensen, Miller et al., 2003). Cores

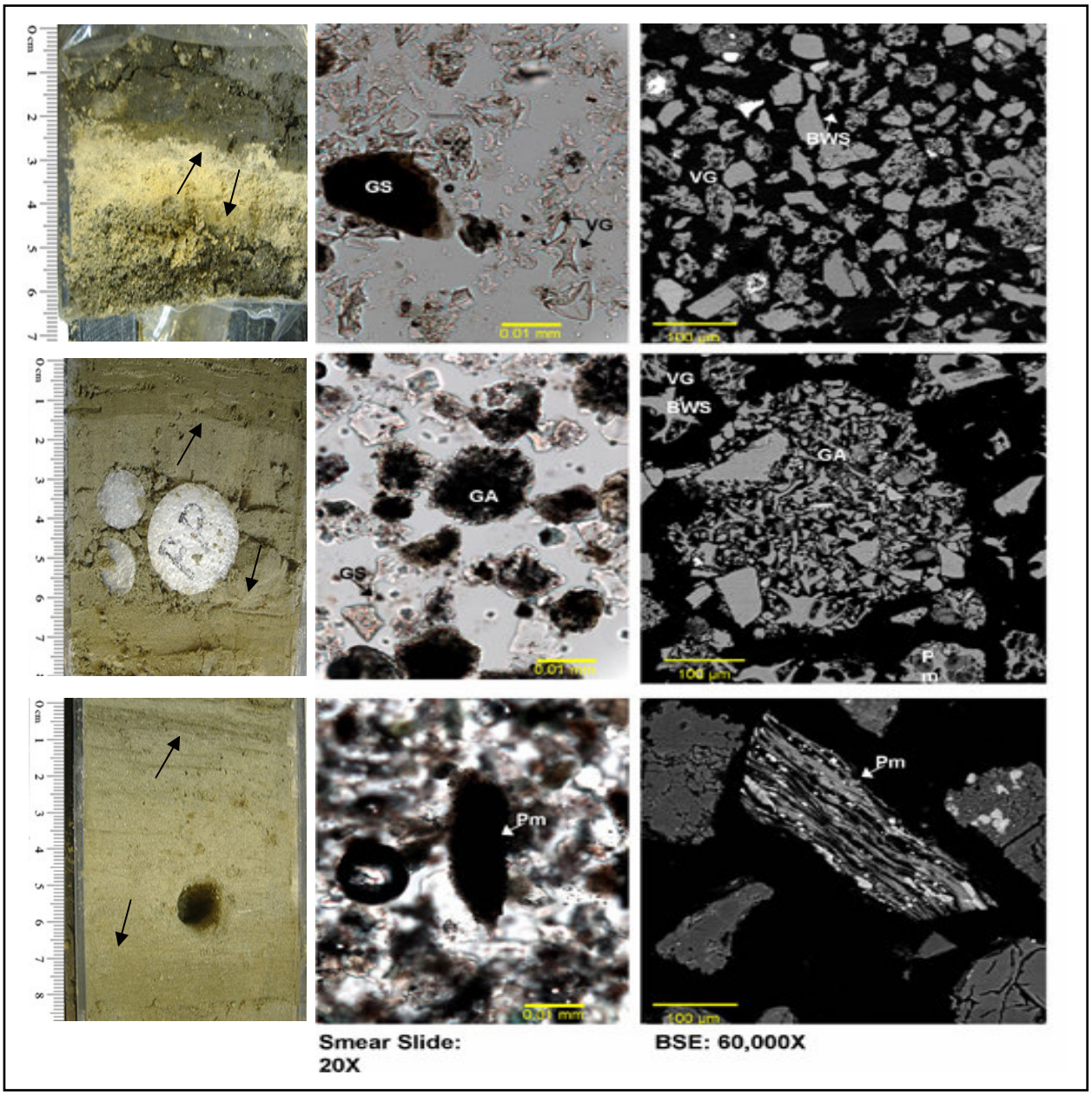

Figure 5: Representative Type 1 ash. Core photographs (left), smear slide (middle), and backscatter electron (right) (BSE) images of three representative ash occurrences for Leg 201 cores. Black arrows point to top and bottom ash layer contacts. From top to bottom, 1227A-13H-2, 146-147.3 cm – represents ash consisting of ~80% volcanic glass in the form of shards (S), bubble wall shards (BWS), and vesicular glass (VG); 1228A-9H-1, 97-101.7 cm – represents ash consisting of vesicular glass (VG), as well as a large glassy aggregate (GA), which consist of various types of glass morphologies; and 1229A-14H-5, 50-55.6 cm – represents ash consisting of ≥ 15% pumice (Pm), as well as ≥ 5% volcanic glass.

from this site contain one Type 1 layer (1.3 cm), two Type 2 layers (0.5 & 1.3 cm's), and nine Type 3 layers (Table 4). In addition to these layers and accumulations twelve layers have suffered diagenesis, resulting in the presence of dolomite (≥10%), with most of these layers containing > 25% dolomite (Table 4). In the absence of diagenesis these layers would be Type 1 layers. The Type 1 layer for this site consists of approximately 85-90% volcanic glass with 5-10% quartz and feldspar (no mafic minerals are present) and there is no rounding of grains and no biogenic component present (Fig. 5 and Table 3). This layer is shown in the stratigraphic section (Fig. 6) as occurring in Miocene sediments, whereas the two secondary layers occur in Pliocene sediments, the ash accumulations occur predominantly within Pleistocene sediments and within one Holocene, one Pliocene, and two Miocene layers as well. The diagenetically altered ash layers occur within Pliocene and Miocene sediments, with the exception of one Holocene layer.

Site 1228 Ash Layers

Site 1228 is located on the Peru shelf at the southeastern edge of the Salaverry Basin (Fig. 1) at a water depth of 252 m (Pouclet et al., 1990; D'Hondt, Jorgensen, Miller et al., 2003).

Table 4
Type 2 through Type 4 ash table.

TYPE 2 LAYERS		TYPE 3 LAYERS		TYPE 4 LAYERS	
Core-Section, Interval (cm)	AGE	Core-Section, Interval (cm)	AGE	Core-Section, Interval (cm)	AGE
Site 1227		**Site 1227**		**Site 1227**	
2H-CC, 22.5 - 23	Pliocene	1H-2, 5.7	Holocene	1H-4, 56	Holocene
3H-1, 116-117.3	Pliocene	1H-2, 110.4	Pleistocene	4H-5, 73	Pliocene
		1H-4, 56	Pleistocene	4H-6, 29.3	Pliocene
		1H-4, 63	Pleistocene	4H-6, 87	Pliocene
		1H-4, 78	Pleistocene	5H-1, 14	Pliocene
		2H-1, 5.8	Pleistocene	6H-3, 135	Pliocene
		3H-1, 62.2	Pliocene	6H-3, 137.3	Pliocene
		11H-1, 78.5	Miocene	7H-1, 14	Pliocene
		12H-1, 82.5	Miocene	7H-1, 150	Pliocene
				7H-2, 3	Miocene
				7H-2, 6	Miocene
				13H-3, 7-105	Miocene
Site 1228		**Site 1228**		**Site 1228**	
1H-1, 98.5 - 99.3	Holocene	2H-4, 111.2 - 111.4	Pleistocene	5H-5, 134 - 150	Pleistocene
1H-1, 121.8 - 122.6	Holocene	2H-4, 131.7	Pleistocene	6H-1, 84	Pleistocene
1H-2, 7.8 - 8.3	Holocene	2H-4, 138.6	Pleistocene	7H-1, 27.5 - 31.7**	Pliocene
2H-3, 122.5 - 123.5	Pleistocene	2H-5, 28 - 30	Pleistocene	7H-3, 117 - 135	Pliocene
2H-6, 121.1 - 121.6	Pleistocene	2H-5, 29.8*	Pleistocene	7H-4, 10 - 14.8	Pliocene
3H-5, 121 - 124.5	Pleistocene	2H-7, 33.3 - 36	Pleistocene	7H-4, 126	Pliocene
3H-5, 35.3 - 38.3	Pleistocene	3H-3, 14 - 14.5	Pleistocene	8H-1, 123	Pliocene
3H-5, 106.8 - 107.4	Pleistocene	5H-2, 122 - 131	Pleistocene	9H-1, 62 - 70**	Pliocene
3H-5, 112.5 - 113.5	Pleistocene	6H-4, 4	Pleistocene	9H-1, 80.5 - 93.5**	Pliocene
3H-6, 149.3 - 150	Pleistocene	6H-4, 14 - 24	Pleistocene	9H-1, 73 - 78.5	Pliocene
3H-7, 0-2	Pleistocene	6H-4, 80	Pleistocene	9H-2, 112.7	Pliocene
4H-6, 84 - 85	Pleistocene	6H-6, 60	Pleistocene		
5H-2, 110 - 121.5	Pleistocene	Dispersed throughout the rest of this core.	Pliocene		
5H-2, 131 - 136	Pleistocene				
5H-5, 70 - 134	Pleistocene				
6H-1, 46	Pleistocene				
6H-1, 77.5 - 82	Pleistocene				
6H-4, 0 - 14	Pleistocene				
7H-1, 26 - 35	Pliocene				
7H-5, 84.5 - 87.2	Pliocene				
7H-6, 8-12	Pliocene				
7H-6, 136.5	Pliocene				
8H-1, 87.5	Pliocene				
8H-2, 23.8	Pliocene				
8H-5, 36	Pliocene				
8H-5, 41	Pliocene				
8H-5, 48.3	Pliocene				
8H-6, 81.5	Pliocene				

Table 4 continued

TYPE 2 LAYERS		TYPE 3 LAYERS		TYPE 4 LAYERS	
Core-Section, Interval (cm)	AGE	Core-Section, Interval (cm)	AGE	Core-Section, Interval (cm)	AGE
Site 1229		**Site 1229**		**Site 1229**	
1H-2, 68 - 72.4	Holocene	1H-2, 98 - 99.6	Holocene	5H-4, 115 - 117	Pleistocene
2H-3, 117.2	Pleistocene	2H-6, 7 - 16	Pleistocene	6H-3, 26.2 - 28	Pleistocene
2H-5, 133 - 135	Pleistocene	2H-6, 77 - 80 +	Pleistocene	6H-3, 55 - 65	Pleistocene
2H-6, 0 - 7	Pleistocene	3H-6, 142 - 146	Pleistocene	10H-5, 44 - 52	Pleistocene
2H-6, 17.5 - 19*	Pleistocene	5H-6, 20 - 38	Pleistocene	10H-5, 52 - 59	Pleistocene
2H-6, 21.3 - 22.5*	Pleistocene	8H-1, 40 - 55	Pleistocene	11H-4, 28 - 33.5	Pleistocene
2H-6, 75.5 - 77	Pleistocene	8H-1, 86.5*	Pleistocene	11H-5, 85 - 87	Pleistocene
2H-7, 9 - 34	Pleistocene	8H-1, 83.5 - 84*	Pleistocene	11H-5, 124**	Pleistocene
2H-7, 38.5 - 41*	Pleistocene	8H-1, 94 - 96	Pleistocene	11H-6, 3 - 5	Pleistocene
3H-1, 65 - 94	Pleistocene	8H-1, 125	Pleistocene	11H-6, 35 - 36	Pleistocene
3H-1, 123, 135	Pleistocene	8H-2, 90 - 130	Pleistocene	12H-4, 65.5 - 73.5	Pleistocene
3H-6, 83 - 88.8	Pleistocene	8H-2, 145 - 149	Pleistocene	13H-CC, 15 - 16	Pleistocene
5H-4, 71 - 77	Pleistocene	9H-4, 81 - 88+	Pleistocene	14H-3, 111.8 - 112.4*	Pleistocene
8H-3, 111.5 - 113*	Pleistocene	12H-5, 43.5 - 56.5	Pleistocene	14H-4, 97 - 98	Pleistocene
9H-2, 104 - 114	Pleistocene	12H-6, 43.4 - 43.6	Pleistocene	14H-4, 98 - 104.5	Pleistocene
9H-2, 116 - 129	Pleistocene	14H-1, 42 - 56.5	Pleistocene	14H-4, 132(134)-137.	Pleistocene
9H-2, 129 - 131.5	Pleistocene	14H-3, 126.5 - 134.5	Pleistocene	14H-5, 43.5 - 46.5**	Pleistocene
9H-2, 131.5 - 134	Pleistocene	14H-4, 68 - 78.5	Pleistocene	14H-5, 46.5 - 50	Pleistocene
9H-2, 134 - 136	Pleistocene	14H-4, 141.4 - 141.5	Pleistocene	14H-5, 56 - 60.5	Pleistocene
9H-4, 21 - 30	Pleistocene	14H-5, 116.5 - 122.5	Pleistocene	14H-5, 62.2 - 86.7	Pleistocene
9H-4, 51 - 53	Pleistocene	14H-CC, 20 - 32	Pleistocene	14H-5, 124 - 136	Pleistocene
9H-4, 58*	Pleistocene	18H-1, 97 - 100	Pliocene	14H-6, 68.5 - 72.6	Pliocene
9H-4, 65 - 66*	Pleistocene	18H-3, 6(4) - 15	Pliocene	18H-2, 127 - 128.8	
9H-4, 68 - 72+	Pleistocene	18H-3, 122 - 124	Pliocene		
9H-4, 88 - 92	Pleistocene				
9H-4, 110 - 115	Pleistocene				
9H-4, 111 - 111.5*	Pleistocene				
9H-4, 117.5 - 120	Pleistocene				
9H-4, 118.8*	Pleistocene				
10H-3, 40 - 41	Pleistocene				
11H-3, 2 - 6.5	Pleistocene				
11H-3, 30 - 32	Pleistocene				
11H-3, 39.3 - 39.6	Pleistocene				
11H-4, 0 - 7.5	Pleistocene				
11-4, 7.5 - 23.5	Pleistocene				
11-4, 73 - 75	Pleistocene				
11-4, 77.5 - 81	Pleistocene				
11-5, 63 - 66	Pleistocene				
11-5, 50 - 60	Pleistocene				
11-5, 132.5 - 134	Pleistocene				
11-5, 68.5 - 69	Pleistocene				
11-5, 69 - 85	Pleistocene				
11-5, 107.5 - 115.5	Pleistocene				
11-6, 0 - 3	Pleistocene				

Table 4 continued

TYPE 2 LAYERS	AGE	TYPE 3 LAYERS	AGE	TYPE 4 LAYERS	AGE
Core-Section, Interval (cm)		Core-Section, Interval (cm)		Core-Section, Interval (cm)	
Site 1229					
11H-6, 5-9	Pleistocene				
11H-6, 9 - 11.3	Pleistocene				
11H-6, 11.3 - 11.5	Pleistocene				
11H-6, 13.5 - 15[++]	Pleistocene				
11H-6, 15 - 16.5	Pleistocene				
11H-6, 29.5 - 35	Pleistocene				
11H-6, 39 - 40	Pleistocene				
11H-6, 40 - 42	Pleistocene				
11H-6, 114.1 - 114.3	Pleistocene				
12H-1, 116 - 126.5	Pleistocene				
12H-4, 31 - 34.5	Pleistocene				
12H-4, 32.7*	Pleistocene				
12H-6, 33 - 35	Pleistocene				
12H-6, 45 - 50.5	Pleistocene				
12H-6, 74.5 - 79.5	Pleistocene				
13H-4, 0 - 3	Pleistocene				
13H-4, 3 - 4	Pleistocene				
13H-4, 77.5 - 86.5	Pleistocene				
14H-1, 85 - 88.2	Pleistocene				
14H-1, 120.5 - 124.5	Pleistocene				
14H-3, 108.5 - 111.8	Pleistocene				
14H-4, 48 - 49	Pleistocene				
14H-4, 78.5 - 86	Pleistocene				
14H-4, 139.5 - 141.4	Pleistocene				
14H-4, 146.5 - 150	Pleistocene				
14H-5, 0 - 19.5	Pleistocene				
14-5, 19.5 - 24	Pleistocene				
14-5, 25 - 27	Pleistocene				
14-5, 27 - 30.5[♦]	Pleistocene				
14-5, 30.5 - 32.5[♦]	Pleistocene				
14-5, 32.5 - 43.5[♦]	Pleistocene				
14-5, 86.7 - 113.7	Pleistocene				
14-5, 122.5 - 123	Pleistocene				
14-6, 9.5 - 25	Pleistocene				
14-6, 30 - 33.5	Pleistocene				
14-6, 36 - 36.3	Pleistocene				
14-6, 58.9 - 68.5	Pleistocene				
14-6, 72.7	Pleistocene				
14-6, 93.5 - 95.2	Pliocene				
18-1, 74(78)-91(97)	Pliocene				
18-1, 98	Pliocene				
18-2, 116.5 - 117.2	Pliocene				

Table 4 continued

TYPE 2 LAYERS	AGE	TYPE 3 LAYERS	AGE	TYPE 4 LAYERS	AGE
Core-Section, Interval (cm)		Core-Section, Interval (cm)		Core-Section, Interval (cm)	
Site 1229					
18-2, 128.8 - 130					
18-2, 137.8 - 138.5					
18-3, 1.2♦♦	Pliocene				
18-3, 124 - 125	Pliocene				
18-3, 125 - 131.5	Pliocene				
18-3, 131.5 - 135	Pliocene				

*= pod, **= borderline (10-15% biogenics), += discontinous,
++= laminae set, ♦= clay (hard to tell biogenic or volcanogenic percent), ♦♦= lens.
Inclined layers have values in parentheses representing the slanted end of the contact.

Cores from this site contain 52 Type 1 layers, three of which are borderline and 38 have been analyzed for whole rock geochemistry, (layer thickness ranges from 0.5 to 13.5 cm's: Table 3). There are also 28 Type 2 ash layers, eight of which contain some dolomite (layer thickness ranges from 0.7 to 14cm's). Layers containing ash accumulations are dispersed sporadically within Pleistocene sediments and are dispersed throughout the entire Pliocene cored sections. In addition eleven Type 4 layers occur sporadically in Cores 5H through 9H (Table 4). Type 1 ash layers for this site consist mostly of quartz and feldspars (~85% - 90%). They contain, on average, 0-2% mafic, pleochroic minerals (biotite or hornblende) and 0–5% volcanic glass (with the exception of layers in sections 9H-1, 69.8 – 72 cm (50% volcanic glass), 11H-2, 50.2-52.3 cm (80% volcanic glass), 11H2-52.3-55 cm (75% volcanic glass), 11H-2, 55-56.6 cm (30% volcanic glass), and 11H-2, 59-60.6 cm (75% volcanic glass)). These layers also contain varying amounts of pumice (0 to 90%) and 1-3 % biogenic material. In general these layers contain less than 1% rounded quartz (with the exception of 10 layers that have 1-2 % round quartz and one layer that has 3-5 % rounded quartz). Seven of the Type 1 layers have no round quartz, two of which contain 50% and 70% volcanic glass, four with high pumice (40-80%), and one with low glass and pumice percent (Fig. 5 and Table 3). Type one ash occurs within Pliocene sediments (Fig. 6), whereas Type 2 ash layers occur within Holocene, Pleistocene, and Pliocene sediments Type 3 and 4 layers occur within Pleistocene and Pliocene sediments.

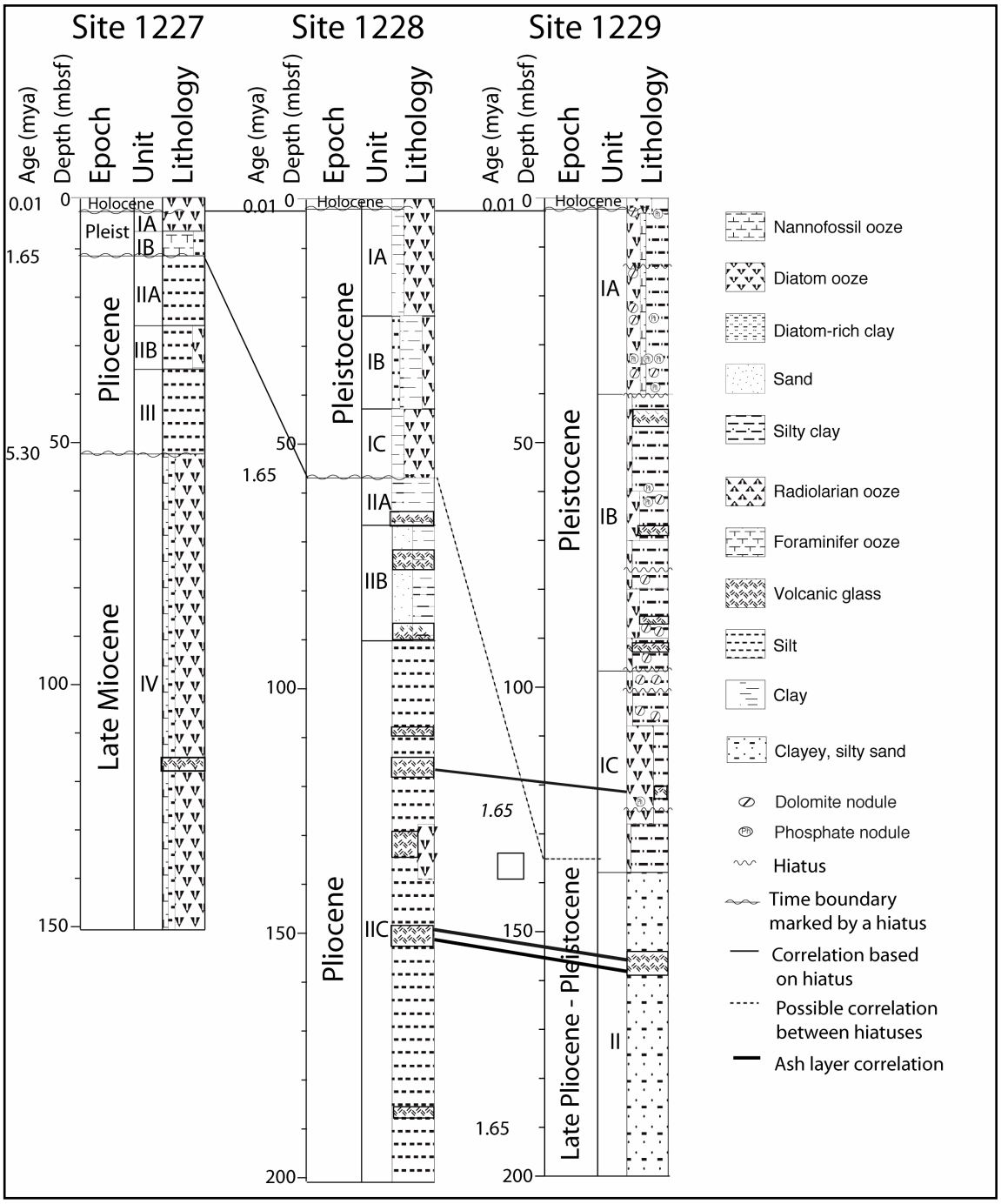

Figure 6: Stratigraphic sections for Leg 201 sites. Lightweight tie line represents the correlation between hiatuses. Heavyweight tie line represents the correlation between ash layers.

Site 1229 Ash Layers

Site 1229 is located on the Peru Shelf at the southeastern edge of the Salaverry Basin slightly northwest of Site 1228 (Fig. 1: Pouclet et al., 1990; D'Hondt, Jorgensen, Miller et al., 2003). This site is the most landward site of the three sites in this study region and has a water depth of 150.5 m (D'Hondt, Jorgensen, Miller et al., 2003).

The cores from this site contain 15 Type 1 ash layers (eight of which are borderline) and 14 layers have been analyzed for whole rock geochemistry. In addition there are six Type 1 ash laminae (≤ 1 mm thick) (Table 3). There are 92 Type 2 layers (nine pods, one lens, and one laminae set), 24 Type 2 ash occurrences, two of which are pods and 23 layers that contain varying amounts of dolomite (Table 4). The Type 1 layers for this site consist mostly of quartz and feldspars (85-92%). They contain, on average, 0-2% mafic, pleochroic minerals (biotite or hornblende) and 0–3% volcanic glass (with the exception of a layer in Section 3H-3, 50–50.5 cm (75% glass)). These layers also contain varying amounts of pumice (0 to 60%) and 0-3 % biogenic material. In general, these layers contain 0-3% rounded quartz (Table 3 and Fig. 5). Type 1 layers are shown in the stratigraphic section (Fig. 6) as occurring within Pleistocene and Pliocene sediments, whereas Type 2 ash layers occur within Pleistocene, and Pliocene sediments, with the exception of one Holocene layer. Type 4 layers occur within Pleistocene sediments with the exception of one layer (Core 1229A-18H-2, 127-128.8 cm (~138.4 mbsf)) that occurs just below the Pleistocene-Pliocene boundary.

Glass Geochemistry of Type 1 Layers

The geochemical analysis of glass shards has been conducted for a select group of ash layers from each Leg 201 site. The analyses of at least ten glass shards within each ash layer has been attempted; however, fewer analyses were conducted for some layers due to the very fine-grained nature of some samples and the plucking of grains during the polishing of the microprobe mounts. The results of these analyses are displayed on TAS and potassium versus silica (K_2O vs. SiO_2) plots (Figs. 7 and 8) for the full set of glasses analyzed and the average value for each ash layer. Average glass values are presented to display the geochemical patterns more clearly.

Overall, Leg 201 glasses display predominantly rhyolitic ($\geq$ 70 wt % SiO_2) chemical compositions (Table 5) and plot mostly in the subalkaline (tholeiitic) series on the TAS diagram (Fig. 7). However, two samples have low silica compositions (most likely due to hydration of glass samples, indicated by low total values), four samples have trachyte – trachydacitic compositions, and one sample has a dacitic composition (Fig. 7 and Table 5). Additionally, the dacitic sample and one other sample (which falls on the boundary between dacite and rhyolite) have very low alkali concentrations (< 4 wt %) and two of the rhyolitic samples have very high silica values (> 80 wt %). This is not displayed for the average glass values (Fig. 8), indicating the possible existence of heterogeneous composition among glasses within some ash layers.

Average glass values fall into two distinct compositional groups (the one outlier could be due to analytical error) (Fig. 8), which are not as apparent on the TAS plot for all glass values (Fig. 7). Average glass TAS values are as follows: five samples from Hole 1228A have slightly high total alkali (8.33 – 8.56 wt %) values and slightly low SiO_2 (69.8 – 71.6 wt %) values (group one, Fig. 8), whereas the remaining four Hole 1228A samples and all Holes 1227A and 1229A samples differ in the opposite sense (total alkali values between 7.29 – 8.06 wt % and silica values between 72.9 – 74.2 wt %; group two, Table 5 and Fig. 8). Although the differences in values between the two groups only differ by a small amount, the groups appear distinctly different on the average value TAS plot.

Overall, the rhyolitic glasses plot in the high-K calc-alkaline and shoshonite fields on the K_2O vs. SiO_2 diagram (Figs. 7 and 8), which compliments Pouclet et al., (1990) geochemical evaluation of glasses from within the same region (ODP Leg 112).

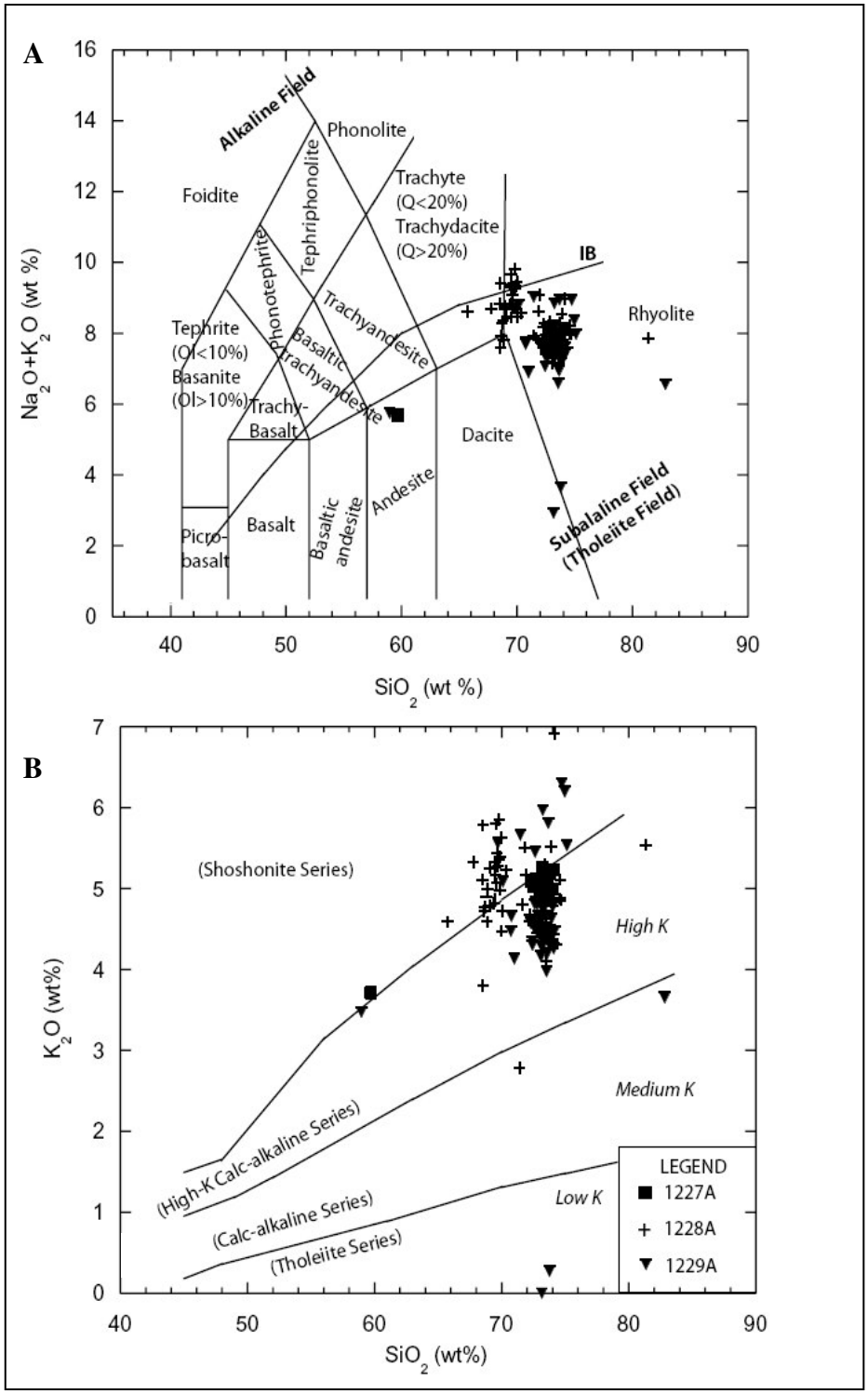

Figure 7: TAS (A) and K_2O vs. SiO_2 (B) plots, glass analyses. The TAS plot displays the Irvine and Baragar (1971) alkaline-subalkaline (tholeiitic) division line (IB). TAS plot values and nomenclature are from Le Maitre et al. (1989) with Rollinson, (1993). The subdivision of the subalkaline field plot values are the average plot value from the compilation of Rickwood (1989) within Rollinson (1993). Nomenclature in parentheses is that of Rickwood (1989) and the nomenclature not in parentheses is that of Le Maitre et al. (1989) within Rollinson (1993).

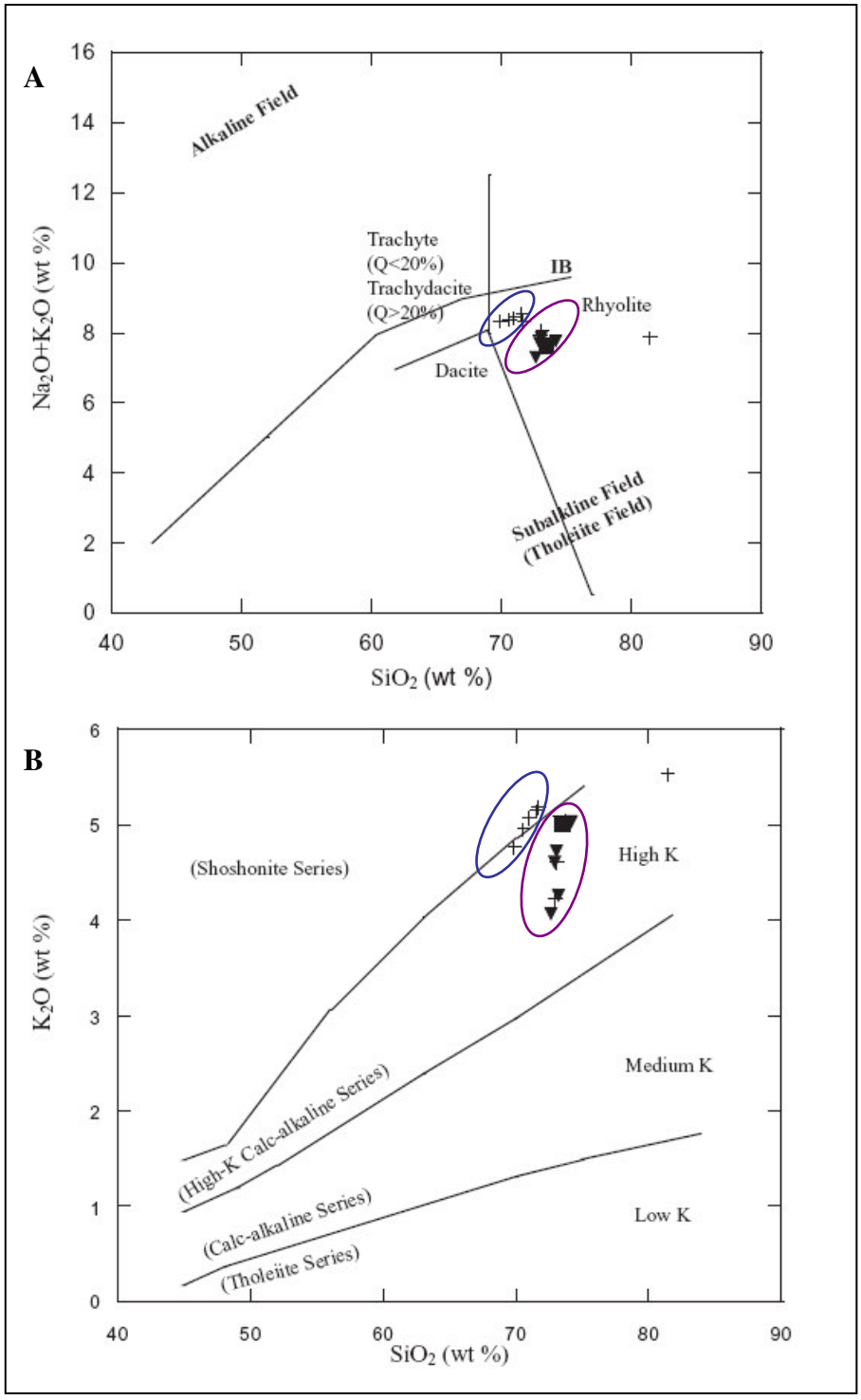

Figure 8: TAS (A) and K_2O vs. SiO_2 (B) plots for average glass values. Symbols are the same as in Figure 7. Blue region = group 1, Purple region = group 2. The TAS plot displays only the subdivision for rhyolites since all values plot within the rhyolitic field (outlier may be due to analytical error, these plot values and nomenclature are from Le Maitre et al. (1989) within Rollinson (1993). The Irvine and Baragar (1971, within Rollinson, (1993)) alkaline-subalkaline division line (IB) is also displayed on this plot. Plot B is the subdivision of the subalkaline field (plot values are the average plot values from the compilation of Rickwood (1989) within Rollinson, (1993)). Nomenclature is the same as that in Figure 7.

Table 5
Average glass analyses.

	WEIGHT PERCENT							
Sample ID	**SiO_2 %**	**Al_2O_3 %**	**FeO %**	**MgO %**	**TiO_2 %**	**P_2O_5 %**	**Na_2O %**	**K_2O %**
1227A-13H-2-146-147.6	73.3	11.6	0.61	0.06	0.12	0.02	2.65	5.04
1228A-9H-1- 97-101.6	71.6	12.7	0.73	0.13	0.14	0.02	3.12	5.20
1228A-11H-2-55-56.6	73.1	13.2	0.53	0.06	0.08	0.06	3.46	4.61
1228A-11H-2-59-60.6	72.9	13.3	0.55	0.09	0.08	0.05	3.67	4.23
1228A-16H-3-96-98.5	81.3	9.6	0.07	0.01	0.10	0.05	2.33	5.54
1228A-16H-4-27-31.5	71.0	13.0	0.94	0.11	0.16	0.03	3.35	5.07
1228A-16H-4-31.5-36	69.8	13.0	1.12	0.14	0.23	0.03	3.56	4.77
1228A-16H-36-40.5	70.5	12.9	0.97	0.12	0.18	0.02	3.44	4.95
1228A-18H-2-88-90	71.5	12.9	1.18	0.14	0.24	0.02	3.41	5.15
1229A-11H-3-7-9	73.2	12.7	0.93	0.08	0.13	0.00	3.27	4.27
1229A-18H-1-1-3	72.7	12.7	0.64	0.09	0.12	0.03	3.22	4.07
1229A-18H-1-44.5-58	72.9	12.4	0.70	0.09	0.12	0.02	3.09	4.61
1229A-18H-2-119-120.5	73.0	12.5	0.69	0.09	0.12	0.02	3.12	4.73
1229A-18H-3-120-121.5	74.2	12.1	0.66	0.06	0.13	0.02	2.71	5.04

	WEIGHT PERCENT				
Sample ID	**CaO %**	**MnO %**	**S %**	**Na_2O+K_2O %**	**Totals**
1227A-13H-2-146-147.6	0.68	0.04	0.10	7.69	94.2
1228A-9H-1- 97-101.6	0.58	0.06	0.03	8.33	94.4
1228A-11H-2-55-56.6	0.64	0.05	0.01	8.06	95.8
1228A-11H-2-59-60.6	0.82	0.04	0.01	7.90	95.8
1228A-16H-3-96-98.5	0.08	0.00	0.03	7.87	99.2
1228A-16H-4-27-31.5	0.53	0.11	0.03	8.42	94.4
1228A-16H-4-31.5-36	0.50	0.11	0.04	8.33	93.3
1228A-16H-36-40.5	0.48	0.10	0.02	8.40	93.7
1228A-18H-2-88-90	0.63	0.06	0.03	8.56	95.3
1229A-11H-3-7-9	0.69	0.09	0.05	7.54	95.3
1229A-18H-1-1-3	0.56	0.05	0.02	7.29	94.2
1229A-18H-1-44.5-58	0.55	0.07	0.03	7.70	94.6
1229A-18H-2-119-120.5	0.53	0.07	0.03	7.85	94.9
1229A-18H-3-120-121.5	0.51	0.06	0.02	7.76	95.5

The average values for the most representative major element oxides are plotted against silica and their trends are displayed on variation diagrams in Figure 9. Additionally, major element oxide regions for glass values from Leg 112, the CVZ, and offshore Central America have been included on the variation diagrams for the purpose of possible source region comparisons.

Major element data for most 1228A glass samples display clear and almost linear trends with increasing SiO_2 content. For example SiO_2 increases as CaO and K_2O increase, and FeO, Na_2O, TiO_2, and MgO decrease with increasing SiO_2 (Fig. 9). Major element data for most 1229A glass samples do not display clear – linear trends with increasing SiO_2 content. The data for these glasses tend to cluster around one particular value as SiO_2 increases, per major element oxide (Fig. 9).

All Leg 201 glasses have major element oxide values that plot on variation diagrams (Fig. 9) within the array of data from Leg 112 samples. All major element oxide values fall within a minimal portion of the array of data of CVZ samples with the exception of TiO_2 and K_2O, which plot largely within the array of data from CVZ samples. In addition, Al_2O_3 plots outside the array of data of CVZ samples (Fig. 9). All Leg 201 glass values plot outside the array of data of Central American samples, with the exception of Na_2O and K_2O, in which a minimal amount of values plot within this data region. It is evident from Figure 9 that Leg 201 glass values concur with Pouclet et al. (1990) values from Leg 112.

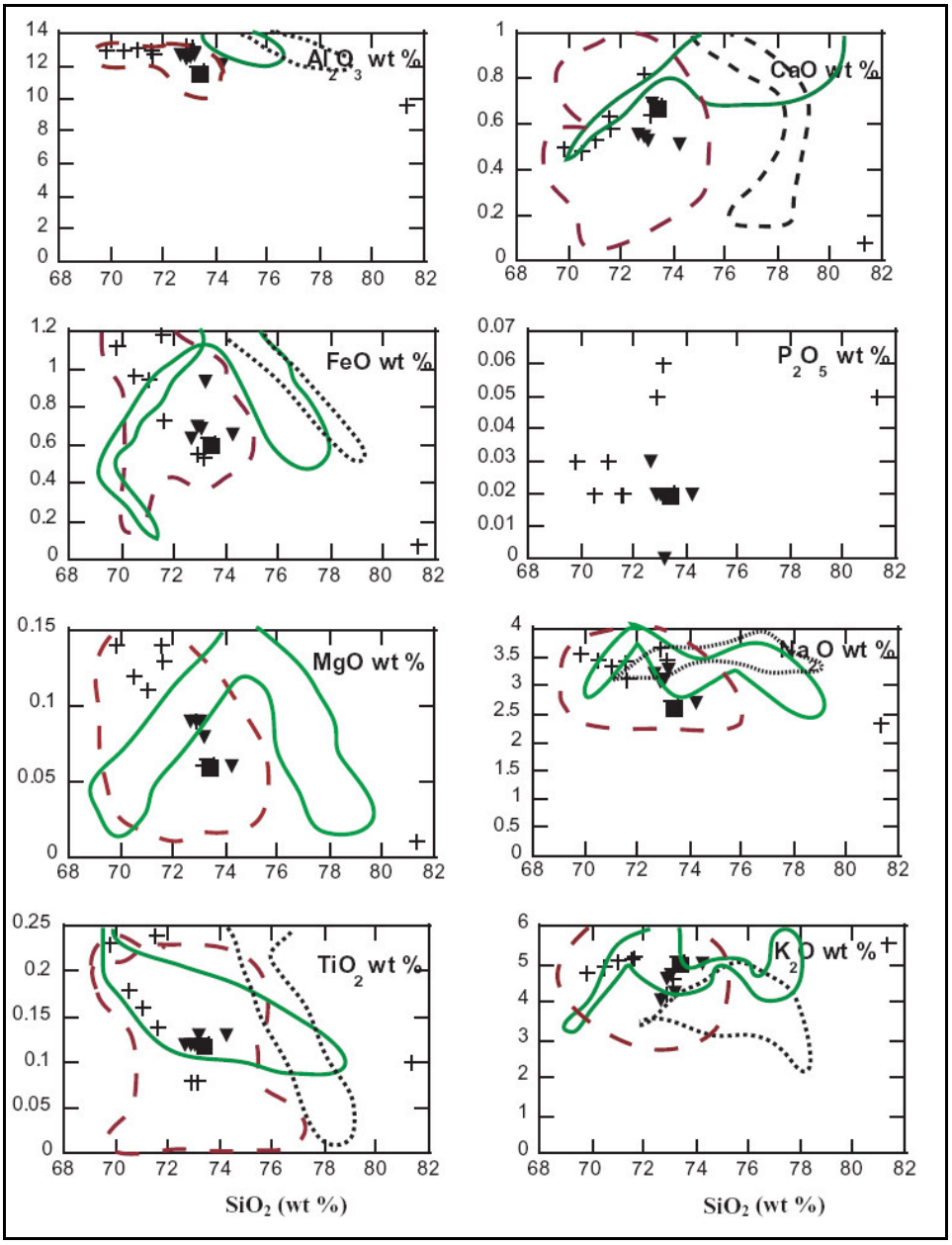

Figure 9: Bivariant plots for major element oxides, average glass values. Leg 201 data are from this study. Representative regions are 1) Green (solid line) = CVZ (data from: Thouret et al., 2002; Siebel et al., 2001; Legros, 2001; Vatin-Perignon et al., 1992; de Silva and Francis, 1989; Thorpe and Francis, 1979), 2) Maroon (dashed line) = Leg 112 (data from: Pouclet et al., 1990), 3) Black (dotted line) = Offshore Central America (data from: Letter and Sparks, 1985). No zones are presented for P_2O_5 wt %, it is plotted here for comparison with whole rock P_2O_5 wt % concentrations. Square = 1227A, crosses = 1228A, inverted triagle = 1229A.

Whole Rock Geochemical Analysis

Major Element Oxides

Leg 201 ash layers have predominantly andesitic to dacitic ($58.8 < SiO_2 < 64.5$ wt %) whole rock chemical compositions (Table 6) and plot in the subalkaline (thoeiilitic) series on the TAS diagram (Fig. 10). However, seven samples have trachybasaltic to basaltic trachyandesitic ($49.5 < SiO_2 < 53.5$ wt %) compositions (these values are most likely due to hydration evidenced by the relatively high (>10 wt %) lost on ignition (LOI) values) and plot in both the alkaline and subalkaline (thoeiilitic) series (Fig. 10). Four of the dacitic samples are distinguished from the rest, in that two of them have high silica values (66.4 and 69.2 wt %), and the other two have the lowest total alkali values (3.79 and 4.55 wt % (these low values are due to low sodium values (1.71 and 2.44 wt % respectively)) (Fig. 10). The Hole 1229A sample with the lowest sodium has a high concentration of silica (68.4 wt %) as well. Additionally, six samples with average silica values lie on, or just above, the boundary between the trachyandesite – trachydacitic fields and andesite - dacite fields (one sample, Hole 1227A) plots well within the trachyandesite field, Fig. 10). All ash layer samples have whole rock compositions that fall in the medium-K or high-K calc-alkaline fields, with the exception of the seven hydrated samples discussed above (Fig. 10).

Table 6
Whole rock (bulk aliquot) geochemical analyses of Leg 201 Type 1 ash layers.

	MAJOR OXIDES											
Sample #	**SiO_2**	**TiO_2**	**Al_2O_3**	**Fe_2O_3**	**MnO**	**MgO**	**CaO**	**Na_2O**	**K_2O**	**P_2O_5**	**LOI**	**Sum**
	wt%	**wt%**	**wt%**	**wt%**	**wt%**	**wt%**	**wt%**	**wt%**	**wt%**	**wt%**	**%**	**%**
Site 1227												
27A-1	63.9	0.31	15.4	1.96	0.03	0.45	3.03	4.29	3.07	0.1	7.2	99.8
Site 1228												
28A-6	62.3	0.65	13.9	3.9	0.06	1.52	5.6	3.2	2.27	0.51	5.9	99.8
28A-10	51.7	0.73	16.8	7.66	0.07	3.25	1.89	2.82	2.85	0.37	11.8	99.9
28A-12	62.6	0.57	14.2	3.34	0.05	2	5.13	3.61	2.32	0.56	5.4	99.8
28A-14	58.9	0.58	13.3	3.35	0.05	2.64	6.36	3.38	2.16	0.58	8.4	99.8
28A-16	59.8	0.59	13.4	3.35	0.05	2.49	6.26	3.44	2.18	0.65	7.6	99.9
28A-19	66.4	0.49	14.0	2.67	0.06	1.12	4.42	3.62	2.64	1.14	3.2	99.8
28A-20	58.8	0.56	14.4	4.71	0.07	1.78	2.05	3.75	3.12	0.42	10.2	99.9
28A-22	60.7	0.44	13.9	3.95	0.05	1.21	4.64	3.81	2.86	1.75	6.5	99.9
28A-23	69.2	0.23	14.9	1.65	0.04	0.61	1.83	4.42	3.78	0.12	3.0	99.9
28A-25	63.4	0.54	14.9	2.73	0.04	1.04	5.63	3.98	2.21	1.52	3.7	99.8
28A-30	63.7	0.64	15.3	3.03	0.04	1.19	4.64	3.93	2.25	0.81	4.3	99.9
28A-32	62.6	0.65	14.9	3.38	0.04	1.34	3.91	3.99	2.32	0.7	6.0	99.9
28A-34	61.1	0.57	13.5	4.05	0.04	1.16	3.98	3.86	2.06	0.87	8.6	99.8
28A-37	64.3	0.6	14.9	2.79	0.04	1.24	3.88	4.2	2.37	0.45	5.0	99.9
28A-38	62.7	0.61	14.7	2.74	0.05	1.3	5.02	4.12	2.3	1.2	5.0	99.9
28A-39	64.3	0.62	15.0	2.79	0.04	1.31	4.01	4.17	2.32	0.45	4.9	99.9
28A-40	63.0	0.6	14.8	2.73	0.05	1.29	4.79	4.15	2.33	1.06	5.0	99.9
28A-45	64.3	0.61	15.1	2.81	0.04	1.27	3.97	4.25	2.41	0.43	4.6	99.9
28A-47	64.4	0.61	15.2	2.73	0.04	1.25	3.87	4.27	2.39	0.34	4.7	99.9
28A-49	64.4	0.63	15.0	2.87	0.04	1.29	3.75	4.17	2.43	0.38	4.8	99.9
28A-50	63.9	0.62	15.1	2.93	0.04	1.35	3.88	4.14	2.48	0.48	4.9	99.9
28A-53	60.5	0.58	14.1	2.78	0.04	1.03	6.99	3.94	2.04	2.65	5.2	99.8
28A-54	61.7	0.59	14.2	2.8	0.04	1.05	6.41	3.94	2.1	2.19	4.8	99.9
28A-56	63.5	0.61	14.7	2.71	0.04	0.99	5.31	3.99	2.15	1.32	4.4	99.8
28A-57	62.5	0.58	14.5	2.66	0.04	1.08	5.53	4.09	2.19	1.57	5.0	99.9
28A-59	61.5	0.66	14.4	2.94	0.05	1.24	6.43	4.03	2.08	1.81	4.4	99.6
28A-60	63.8	0.36	14.5	1.92	0.04	0.85	4.06	4.64	2.53	0.77	6.2	99.8
28A-64	63.0	0.58	14.7	2.77	0.04	1.27	5.03	3.98	2.34	1.14	4.9	99.8
28A-65	61.8	0.59	14.6	2.8	0.05	1.34	5.39	3.95	2.28	1.37	5.4	99.6
28A-67	62.4	0.61	14.7	2.84	0.04	1.27	5.19	3.95	2.36	1.38	5.0	99.8
28A-70	63.0	0.58	14.7	2.87	0.04	1.28	4.66	3.99	2.45	1.06	5.0	99.7
28A-71	62.4	0.59	14.6	2.95	0.04	1.32	4.68	4	2.47	0.97	5.6	99.7
28A-73	62.7	0.59	14.6	2.99	0.04	1.31	4.95	3.99	2.33	1.08	5.0	99.7
28A-75	62.3	0.59	14.1	3.18	0.04	1.46	3.69	4.04	2.31	0.67	7.2	99.7
28A-76	60.3	0.56	14.1	2.71	0.05	1.15	6.55	3.87	2.23	2.19	5.8	99.6
28A-77	63.2	0.59	14.7	2.9	0.04	1.23	4.5	4.05	2.44	0.93	5.1	99.8
28A-80	61.7	0.54	14.2	2.91	0.05	1.19	5.87	3.9	2.29	1.82	5.1	99.7
28A-81	62.9	0.57	14.6	3	0.05	1.27	4.63	4	2.38	0.99	5.3	99.8
28A-82	61.3	0.57	14.2	2.94	0.05	1.2	6.54	3.82	2.18	2.12	4.6	99.6

Table 6 continued

	MAJOR OXIDES											
Sample #	**SiO_2**	**TiO_2**	**Al_2O_3**	**Fe_2O_3**	**MnO**	**MgO**	**CaO**	**Na_2O**	**K_2O**	**P_2O_5**	**LOI**	**Sum**
	wt%	**wt%**	**wt%**	**wt%**	**wt%**	**wt%**	**wt%**	**wt%**	**wt%**	**wt%**	**%**	**%**
Site 1229												
29-1	51.9	0.7	16.3	7.02	0.07	2.8	1.92	2.68	2.57	0.14	13.6	99.7
29-2	58.9	0.7	15.1	5.87	0.07	2.47	3.1	3.33	2.53	0.18	7.2	99.5
29-3	49.5	0.67	14.0	6.24	0.07	2.47	4.13	2.8	2.42	0.25	17.0	99.5
29-4	64.5	0.69	12.5	4.25	0.06	1.53	4.57	2.44	2.11	0.14	7.0	99.8
29-6	53.5	0.79	17.9	6.07	0.08	2.32	2.38	2.56	2.89	0.23	10.2	98.9
29-7	68.4	0.85	11.6	4.23	0.06	1.09	2.48	1.71	2.08	0.17	6.6	99.2
29-8	62.5	0.65	13.3	4.31	0.07	1.72	4.98	3.13	2.21	0.26	6.4	99.5
29-9	60.9	0.55	13.1	3.19	0.05	1.53	6.53	3.59	2.25	1.8	6.2	99.7
29-11	60.0	0.6	13.4	3.41	0.05	1.42	5	4.16	2.25	0.76	8.0	99.1
29-12	61.7	0.63	14.0	3.28	0.06	1.35	5.37	3.86	2.34	1.22	5.8	99.5
29-13	61.5	0.59	13.9	3.41	0.05	1.35	4.52	3.97	2.22	0.73	7.4	99.7
29-14	63.9	0.63	13.6	3.56	0.06	1.43	5.17	3.47	2.39	0.46	5.6	100.3
29-16	62.3	0.57	14.0	3.04	0.06	1.23	5.65	4.02	2.2	1.36	5.0	99.4
29-18	49.1	0.7	15.8	7.63	0.09	2.9	2.07	2.72	2.75	0.16	16.0	99.9
29-19	49.5	0.68	16.3	7.86	0.08	2.74	1.45	2.65	2.67	0.07	15.8	99.8
29C-21	51.3	0.74	15.5	6.84	0.07	3.12	2.56	3.25	2.14	0.24	14.4	100.2
2.90E-21	60.9	0.67	14.1	5.07	0.07	2.19	4.38	3.24	2.12	0.22	7.0	100.0

Table 6 continued

	TRACE ELEMENTS												
Sample #	**Sc**	**V**	**Co**	**Ni**	**Rb**	**Sr**	**Y**	**Zr**	**Nb**	**Ba**	**La**	**Ce**	**Nd**
	ppm	**ppm**	**ppm**	**ppm**	**ppm**	**ppm**	**ppm**	**ppm**	**ppm**	**ppm**	**ppm**	**ppm**	**ppm**
Site 1227													
27A-1	2	39	1.90	<20	101.9	745	5.7	132	6.0	822	26.4	46.1	19.1
Site 1228													
28A-6	11	80	7.20	< 20	82.8	384	26.0	161	8.8	495	26.3	53.4	24.8
28A-10	17	171	17.60	31.00	124.8	200	16.9	111	8.6	409	19.4	39.9	17.8
28A-12	10	69	6.30	23.00	79.7	424	21.0	151	8.0	534	24.8	51.3	23.4
28A-14	10	75	6.50	< 20	78.4	430	21.7	138	8.0	506	25.4	51.5	23.5
28A-16	10	72	6.40	< 20	77.9	441	22.5	169	8.0	511	26.1	52.1	23.7
28A-19	10	64	5.70	< 20	97.0	469	27.7	264	7.6	971	28.4	60.0	25.3
28A-20	10	106	14.80	40.00	142.9	319	26.1	113	9.8	585	28.4	76.9	32.3
28A-22	11	69	8.50	29.00	105.6	508	34.3	127	7.5	624	27.8	59.6	25.3
28A-23	4	21	1.70	< 20	134.9	481	9.6	132	7.0	870	27.5	57.9	23.3
28A-25	13	80	4.40	< 20	72.4	590	28.6	201	6.5	642	26.2	59.6	26.2
28A-30	13	101	4.40	< 20	72.8	514	24.9	206	7.9	656	23.0	53.0	25.0
28A-32	12	134	6.10	< 20	76.3	458	22.1	169	7.9	589	22.0	49.9	22.1
28A-34	11	137	5.70	48.00	68.5	416	26.1	189	6.9	527	23.3	54.2	26.0
28A-37	10	80	5.60	< 20	75.6	428	20.2	162	7.3	609	22.7	48.2	22.3
28A-38	16	85	5.20	< 20	75.4	543	27.0	187	7.9	605	26.9	55.8	27.0
28A-39	10	86	5.90	< 20	79.8	463	21.7	177	8.1	597	24.5	52.6	23.6
28A-40	14	83	5.30	20.00	78.6	505	24.9	173	7.5	617	26.8	54.3	24.4
28A-45	11	92	5.50	< 20	81.2	447	21.2	159	8.1	613	25.2	52.1	23.3
28A-47	11	89	5.70	< 20	80.4	448	20.4	158	8.2	622	24.2	49.6	22.7
28A-49	11	94	5.80	< 20	80.4	424	19.5	155	8.1	656	23.8	49.0	22.9
28A-50	11	92	6.10	< 20	84.2	454	21.4	157	8.3	622	25.4	52.7	23.7
28A-53	13	115	4.50	< 20	65.6	602	31.2	213	7.1	621	27.5	62.2	27.6
28A-54	12	112	4.80	< 20	68.6	602	32.1	223	7.6	574	29.3	66.4	29.3
28A-56	12	101	4.10	< 20	70.5	539	30.3	237	8.0	595	29.3	65.1	28.7
28A-57	12	103	4.30	28.00	71.5	533	27.8	210	7.7	579	24.9	56.2	24.4
28A-59	13	80	5.10	32.00	68.7	580	30.7	212	8.3	596	33.2	67.2	32.2
28A-60	7	48	3.00	22.00	86.9	434	18.1	120	6.8	619	25.0	50.2	22.1
28A-64	11	70	4.30	< 20	77.0	478	24.2	153	7.7	764	25.5	50.8	24.7
28A-65	12	75	5.60	< 20	80.8	532	27.6	182	8.0	609	28.8	58.9	28.1
28A-67	13	81	5.10	< 20	82.7	531	27.9	189	8.0	596	29.7	59.4	28.4
28A-70	12	77	4.70	28.00	85.1	479	23.9	152	8.3	597	26.7	51.8	24.6
28A-71	12	81	4.90	< 20	87.8	487	25.2	162	8.3	605	28.5	56.5	25.5
28A-73	11	78	5.60	20.00	80.4	500	27.3	178	7.9	612	30.2	59.3	29.0
28A-75	10	89	5.60	< 20	85.3	419	21.2	152	8.1	578	25.1	49.7	23.4
28A-76	13	82	4.10	29.00	76.0	579	29.0	188	7.6	586	28.9	58.2	27.6
28A-77	11	74	4.70	< 20	86.4	473	24.0	165	8.3	601	27.9	54.2	26.3
28A-80	12	80	4.20	< 20	79.0	538	27.7	173	7.7	572	29.8	58.9	27.8
28A-81	11	74	5.50	35.00	83.8	465	24.5	184	7.8	582	28.7	56.2	28.1
28A-82	14	76	4.50	< 20	75.9	567	31.2	223	8.1	562	34.1	68.3	30.3

Table 6 continued

	TRACE ELEMENTS												
Sample #	**Sc**	**V**	**Co**	**Ni**	**Rb**	**Sr**	**Y**	**Zr**	**Nb**	**Ba**	**La**	**Ce**	**Nd**
	ppm	**ppm**	**ppm**	**ppm**	**ppm**	**ppm**	**ppm**	**ppm**	**ppm**	**ppm**	**ppm**	**ppm**	**ppm**
Site 1229													
29-1	18	166	17.00	50	128.8	172	17.3	106	7.3	386	17.6	34.2	17.2
29-2	18	116	13.70	25	104.6	263	21.7	106	6.8	563	18.7	38.2	20.1
29-3	16	127	15.20	43	108.1	233	20.6	129	7.9	418	20.2	41.0	20.6
29-4	12	87	9.10	32	83.2	241	24.5	247	11.5	321	27.1	55.6	23.7
29-6	18	143	18.40	34	114.5	216	27.9	164	12.2	400	33.6	71.9	33.0
29-7	13	75	9.70	23	82.7	163	36.2	378	15.3	303	30.7	65.1	30.1
29-8	14	93	12.20	31	79.0	315	24.7	163	8.2	473	23.8	49.8	24.6
29-9	12	83	5.90	24	78.0	495	28.1	161	7.7	586	27.2	55.7	28.8
29-11	12	86	6.10	24	77.8	430	22.1	154	8.4	509	25.3	51.0	25.8
29-12	14	84	5.90	21	79.0	487	28.9	196	8.7	566	29.8	59.5	31.5
29-13	12	79	6.90	28	75.6	410	23.9	165	7.7	502	24.4	49.7	23.8
29-14	12	88	7.10	28	80.0	382	25.9	234	8.5	516	26.1	52.8	28.5
29-16	13	76	6.20	24	71.5	501	30.1	235	7.1	599	29.1	61.5	31.0
29-18	21	165	18.20	35	117.4	178	19.4	107	8.1	329	21.7	44.4	21.7
29-19	20	226	19.60	36	123.2	166	15.6	109	8.1	353	18.5	34.0	18.3
29C-21	19	145	16.90	42	104.4	177	22.0	97	8.5	377	18.9	40.4	19.6
2.90E-21	16	110	10.90	25	88.0	281	22.3	143	7.8	502	20.8	41.0	21.7

Table 6 continued

	TRACE ELEMENTS					
Sample #	**Eu**	**Gd**	**Dy**	**Er**	**Yb**	**Th**
	ppm	**ppm**	**ppm**	**ppm**	**ppm**	**ppm**
Site 1227						
27A-1	0.70	1.49	0.96	0.45	0.51	10.3
Site 1228						
28A-6	1.1	4.67	3.78	2.41	2.49	8.2
28A-10	0.77	3.47	2.93	1.64	1.73	13.9
28A-12	0.96	4.25	3.34	1.97	1.92	9.7
28A-14	1.07	4.09	3.24	2.02	2	8.7
28A-16	1.1	4.45	3.61	2.11	2.04	9.4
28A-19	1.12	4.74	4	2.46	2.49	11.3
28A-20	1.21	5.72	4.52	2.46	2.26	12.0
28A-22	1.04	4.84	4.31	3.12	3.12	9.1
28A-23	0.75	2.66	1.64	0.72	0.75	10.5
28A-25	1.31	5.28	4.25	2.61	2.56	9.1
28A-30	1.09	4.62	3.87	2.25	2.05	9.5
28A-32	0.98	3.9	3.66	2.04	1.9	8.3
28A-34	1.04	4.89	3.77	2.18	2.14	10.3
28A-37	1.08	4.01	3.26	1.9	1.77	8.3
28A-38	1.27	5.17	3.96	2.56	2.42	10.6
28A-39	1.13	4.21	3.45	1.99	1.89	8.4
28A-40	1.14	4.38	3.71	2.31	2.08	8.5
28A-45	1.08	4.08	3.36	1.89	1.82	8.7
28A-47	1.13	3.98	3.28	1.89	1.81	8.3
28A-49	1.03	4.37	3.08	1.76	1.85	9.3
28A-50	1.14	3.92	3.26	1.93	1.84	9.1
28A-53	1.26	5.22	4.45	2.6	2.45	8.7
28A-54	1.44	5.59	4.37	2.55	2.67	12.1
28A-56	1.28	5.32	4.37	2.66	2.39	10.7
28A-57	1.17	4.99	4.02	2.32	2.24	10.3
28A-59	1.38	6.01	4.87	2.86	3.1	11.7
28A-60	1.08	3.59	2.92	1.74	1.88	8.5
28A-64	1.11	4.19	3.72	2.27	2.12	9.8
28A-65	1.34	5.17	4.14	2.24	2.34	11.5
28A-67	1.26	5	4.1	2.38	2.61	10.1
28A-70	1.13	4.83	3.7	1.94	2.19	10.2
28A-71	1.18	4.58	3.98	2.08	2.04	10.8
28A-73	1.38	5.32	4.17	2.51	2.54	10.1
28A-75	1.02	4.12	3.07	1.94	2.01	11.0
28A-76	1.17	4.98	3.82	2.53	2.67	11.0
28A-77	1.14	4.36	3.66	2.2	2.18	10.3
28A-80	1.25	5.08	3.98	2.17	2.45	11.5
28A-81	1.22	4.99	3.57	2.23	2.31	11.3
28A-82	1.45	5.74	4.66	2.56	2.78	12.7

Table 6 continued

	TRACE ELEMENTS					
Sample #	**Eu**	**Gd**	**Dy**	**Er**	**Yb**	**Th**
	ppm	**ppm**	**ppm**	**ppm**	**ppm**	**ppm**
Site 1229						
29-1	0.70	2.69	2.47	1.62	2.09	11.2
29-2	0.93	3.76	3.08	2.07	2.25	10.3
29-3	0.88	3.45	3.09	1.93	2.23	13.0
29-4	1.02	4.18	3.79	2.43	2.55	11.4
29-6	1.56	5.28	4.70	2.89	2.99	13.3
29-7	1.31	5.83	5.49	3.58	3.38	10.4
29-8	1.15	4.48	3.95	2.55	2.33	8.3
29-9	1.24	4.52	3.68	2.38	2.66	8.9
29-11	1.13	4.10	3.40	2.14	1.95	7.8
29-12	1.32	5.10	4.29	2.73	2.52	8.9
29-13	1.06	4.09	3.46	2.28	2.05	8.2
29-14	1.20	4.31	4.32	2.53	2.54	9.8
29-16	1.41	5.23	4.32	2.78	2.68	12.8
29-18	0.92	3.99	3.23	2.02	1.88	10.9
29-19	0.76	2.76	2.47	1.70	1.55	14.1
29C-21	0.86	3.94	3.54	2.37	2.25	11.4
2.90E-21	0.91	3.74	3.75	2.33	2.15	9.9

See Table 8 in Appendix A for sample location within cores

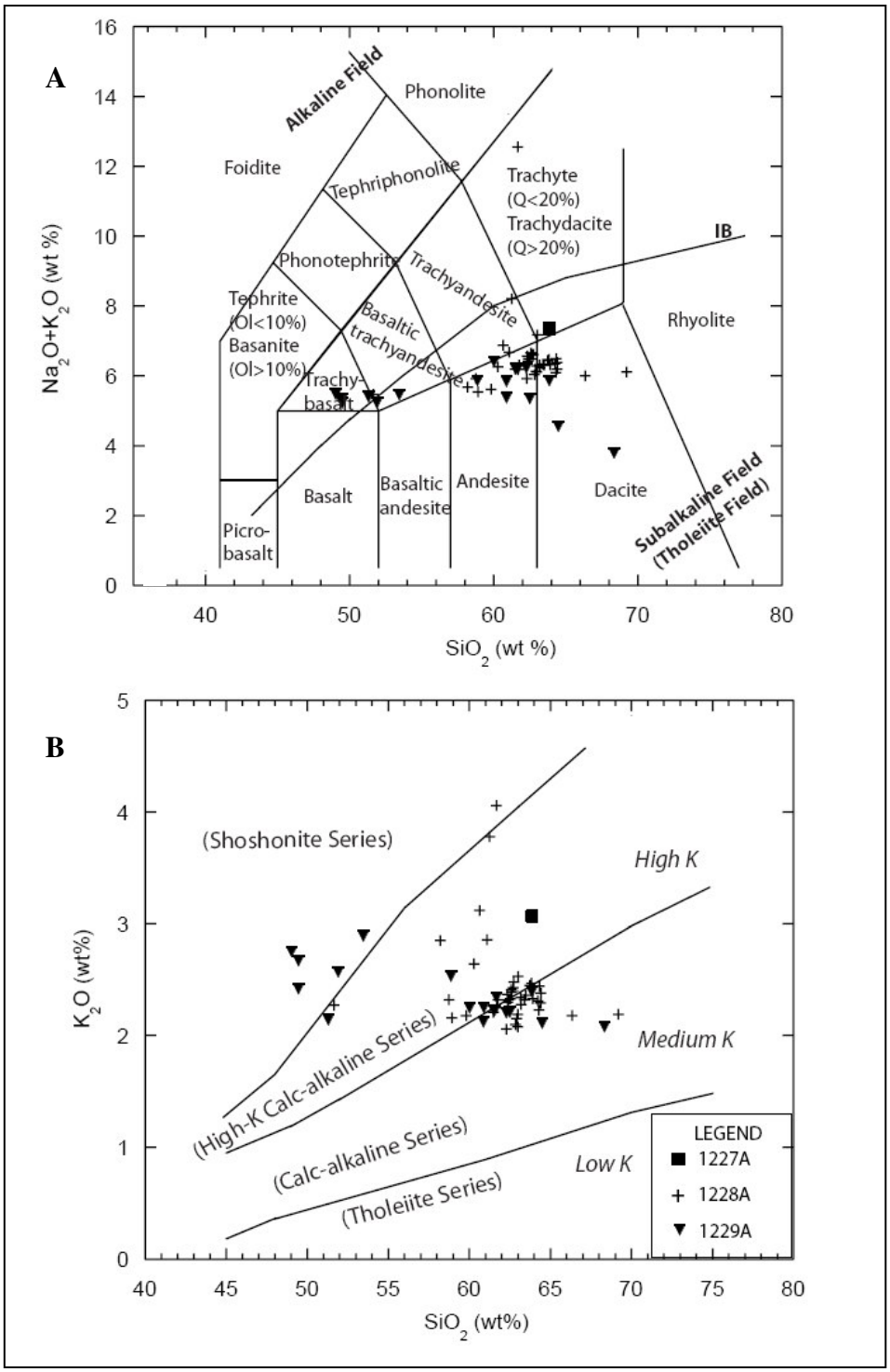

Figure 10: Whole rock TAS (A) and K_2O vs. SiO_2 (B) plots. (A) Displays the Irvine Baranger (1971, within Rollinson, (1993)) alkaline-subalkaline (tholeiitic) division line (IB). (B) The subdivision of the subalkaline field. The plot values and nomenclatures are the same as that of Figures 7 and 8.

The most representative major element oxide values are plotted against silica and their trends are displayed on variation diagrams in Figure 11. Additionally, major element oxide regions for whole rock values from the CVZ, NVZ, and SVZ have been included on the variation diagrams for the purpose of possible source region comparisons.

Some Site 1228 and 1229 samples plot to the left side (low silica) of the variation diagrams as a result of hydration (these samples have high LOI values, Table 6). The intermediate (andesitic and trachyandesitic) and acidic (dacitic and trachytic) samples plot together and display regular and continuous trends with increasing Al_2O_3, Na_2O, K_2O, and TiO_2, as SiO_2 increases for Site 1228 samples. These oxides decrease with increasing SiO_2 for Site 1229 samples, with the exception of TiO_2 whose trend is not apparent. CaO, Fe_2O_3, and MgO decrease as SiO_2 increases for samples from both sites; apparent trends are less obvious for P_2O_5 with increasing SiO_2. Sites 1228 and 1229 samples have P_2O_5 values between 0.12 – 2.65 wt % and 0.10 – 1.36 wt %, respectively (average values are 1.09 and 0.49 wt % respectively). 64% of Site 1228 and 29% of Site 1229 samples have P_2O_5 wt % values that are considerably greater (Table 6 and Fig. 11) than that reported by the United States Geological Survey (USGS) and Le Maitre (1976) (0.15-0.63 wt % P_2O_5) for andesitic to dacitic whole rock standard compositions. The high P_2O_5 values for these samples can possibly be attributed to diagenetic alteration, in the form of secondary apatite and phosphate, since fluoroapatite and phosphate concretions have been documented throughout Leg 201 cores (D'Hondt, Jorgensen, Miller et al., 2003).

The primary volcanological province from which Leg 201 ash layers were erupted can be inferred from the major element oxide plots in Figure 11. Leg 201 samples with intermediate and acidic compositions have major element oxide values that plot predominantly within the CVZ region (Fig. 11) (with the exception of three samples: one 1228A sample plots solely within the NVZ region for Al_2O_3 and Na_2O, one 1229A sample plots entirely within the NVZ region for Fe_2O_3 and Na_2O, and plots outside any region for TiO_2, and the one 1227A sample plots outside any region for TiO_2 as well). However, data from the NVZ overlaps that of the CVZ for all major element oxides with the exception of Fe_2O_3 and MgO (Fig. 11). A minimal portion of the major element oxide values for the samples with intermediate and acidic compositions plot within the SVZ data region, with the exception of CaO, P_2O_5, and Na_2O, in which a larger portion of these values fall within the data set of the SVZ (Fig. 11). Overall, these plots indicate that most Leg 201 ash layers originated primarily from volcanic centers within the CVZ. However, these plots also indicate that some layers may have been erupted from volcanic centers within either the CVZ or NVZ, evidenced by some Leg 201 data values falling within the overlapping CVZ and NVZ data regions displayed in Figure 11.

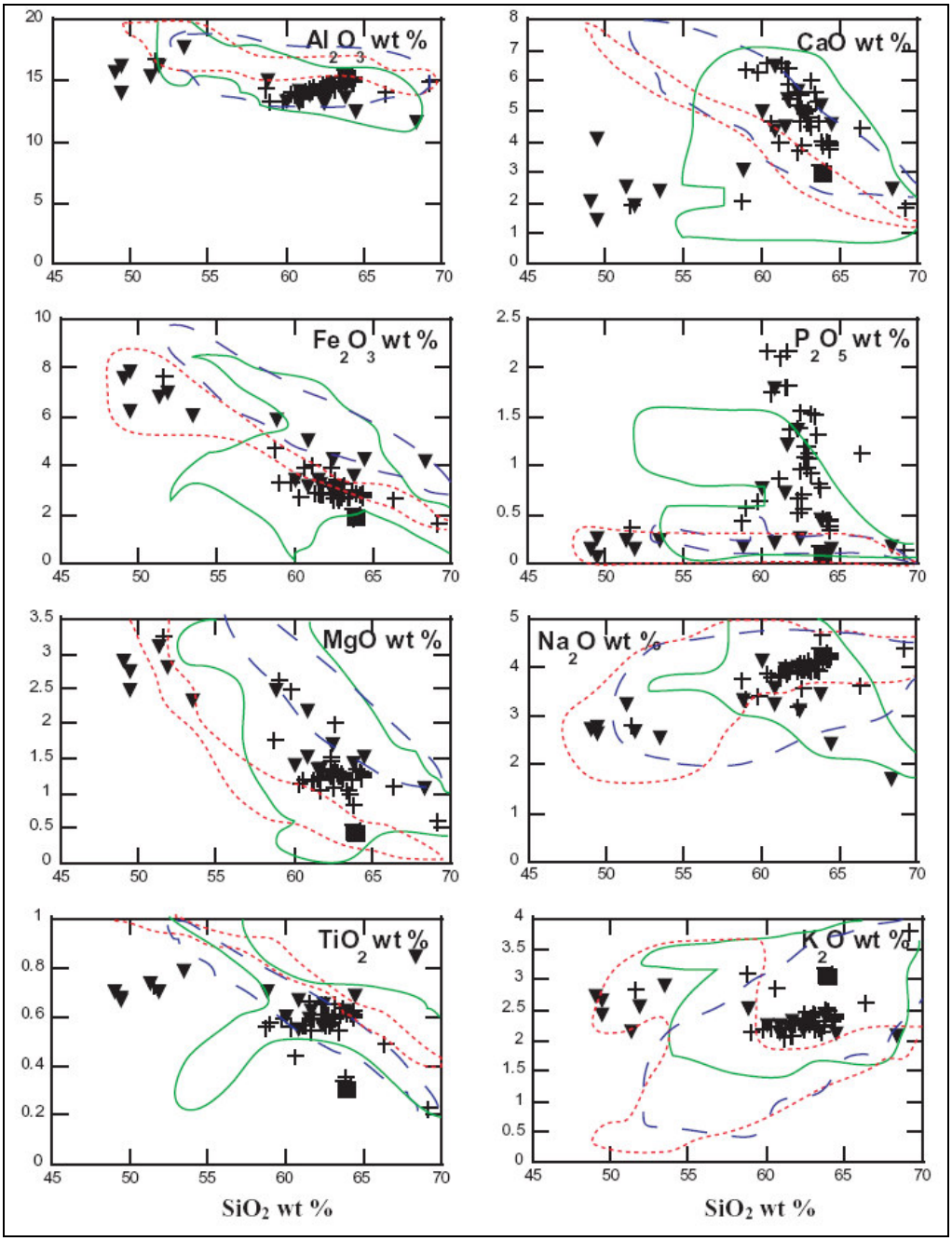

Figure 11: Whole rock major element oxide plots. Whole rock data are from this study. Representative regions are 1) Blue (dashed line) = NVZ (data from: Droux and Delaloye, 1996; Monzier et al., 1999), 2) Green (solid line) = CVZ (data from same sources as Figure 9), 3) Red (dotted line) = SVZ (data from: Gutierrez et al., 2005; Trumbull et al., 1999).

Rare Earth Elements

REE plots are presented for each Andean volcanic zone and for all Type 1 layers (Fig. 12) in order to refine the primary volcanological province deduced from whole rock major element oxide plots. Additionally, these data are presented in order to infer possible formation processes of the magma that generated the ash. The REE have also been utilized to refine possible ash layer correlations between sites.

The REE content for most ash layers, with the exception of two layers, steadily decrease from the strongly enriched light REE (LREE) through Eu. The heavy REE (HREE) are moderately depleted with respect to the LREE and display a nearly flat array (Fig. 12). Eu data suggest plagioclase enrichment in bulk rock ash (e.g. the lack of a distinct Eu anomaly common to lavas with high plagioclase concentrations) (Rollinson, 1993). These REE patterns are most similar to those of the CVZ (Fig. 12). Figure 12 was created based on a compilation of regions and is representative of each region as a whole. However, the REE patterns for some individual study regions may deviate from this average plot. For instance, although the average REE regions for the CVZ plotted in Figure 12 displays a negative Eu anomaly, not all regions within the CVZ display this anomaly (Vatin-Perignon et al., 1992; Richards and Villeneuve, 2001).

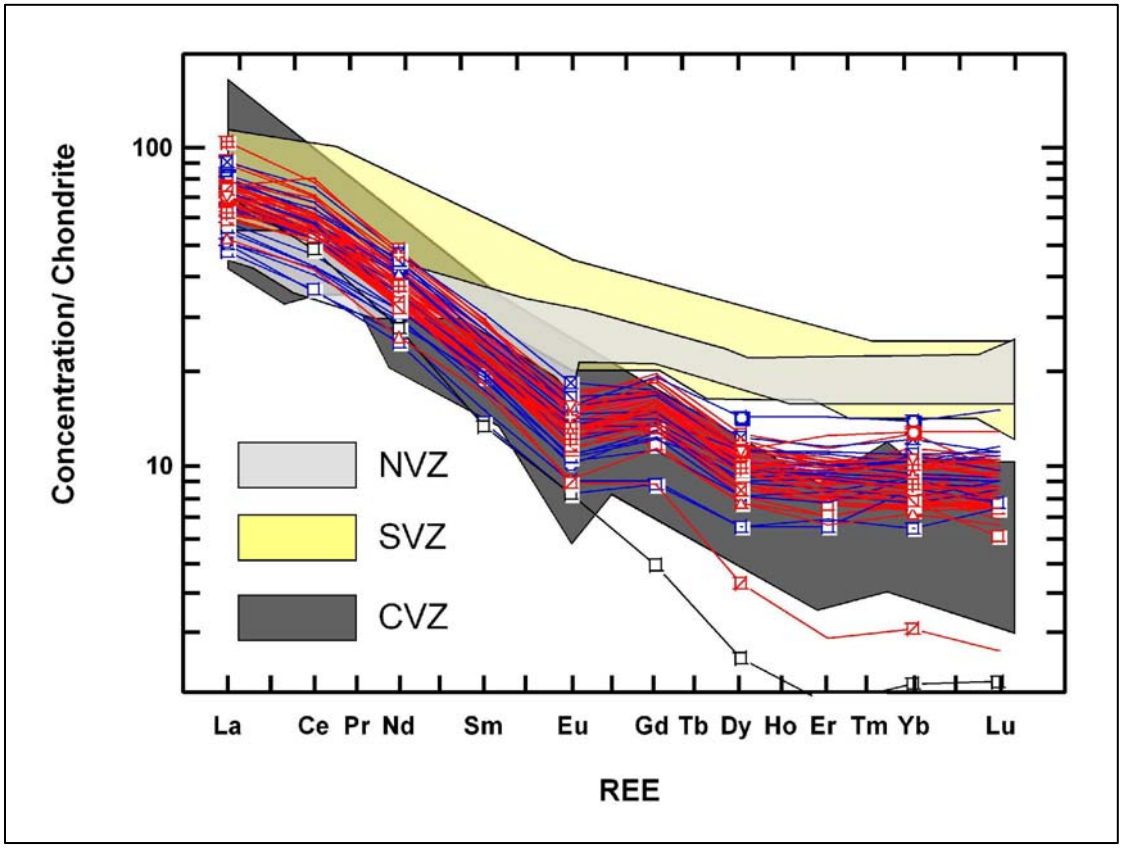

Figure 12: REE geochemical zones for Leg 201 and the three volcanic zones of the Andes. Leg 201 zones are from this study. The SVZ was compiled from (Gutierrez et al., 2005; D'Orazio et al., 2003), the NVZ is from (Droux and Delaloye, 1996), and the CVZ is compiled from (Petrinovic et al., 2005; Matteini et al., 2002; Richards and Villeneuve, 2001; Siebel et al, 2001; Vatin-Perignon et al., 1992; Dostal, Dupuy, and Lefevre, 1977). Red, blue, and black lines are REE plots for Leg 201 ash layers. (Black = 1227, Red = 1228, Blue = 1229).

The overall REE pattern for the SVZ and NVZ are similar to that of the CVZ and Leg 201 ash in that the HREE are depleted with respect to LREE and display a flat array. However, the HREE are enriched relative to the CVZ and Leg 201 ash layers. Based on these data it can be concluded that the ash from Leg 201 have more of an affinity to CVZ type ashes than SVZ and NVZ, which is consistent with the major element oxide data that has been presented for this study.

Chondrite normalized REE patterns are often used to indicate processes occurring during magma generation (Rollinson, 1993; Droux and Delaloye, 1996; Trumbull et al., 1999; Monzier et al., 1999; Dorendorf, et al., 2000; Richards and Villeneuve, 2001; Matteini et al., 2002). As previously noted, the principal magma source for the andesitic volcanoes of the CVZ is believed to be derived from the partial melting of an asthenospheric wedge between the overriding continental South American plate and the descending oceanic Nazca plate (Hanus and Vanek, 1978; Baker and Francis, 1978; Thorpe and Francis, 1979; de Silva and Francis, 1991). Leg 201 ash layers display three distinct REE characteristics. First, the moderate depletion of the HREE with respect to the LREE displayed by all Leg 201 ash layers (Fig. 12) may indicate the occurrence of partial melting of a lower crust or a mantle source with garnet as a residual phase (Rollinson, 1993; Droux and Delaloye, 1996; Trumbull et al., 1999; Monzier et al., 1999; Dorendorf, et al., 2000; Richards and Villeneuve, 2001; Matteini et al., 2002). Alternatively, this REE pattern could indicate the precipitation of garnet from the melt prior to eruption. Additionally, the depletion of middle REE (MREE) with respect to LREE may indicate

the precipitation of amphiboles from the melt. This depletion could indicate the partial melting of a source rock with amphibole as a residual phase (Rollinson, 1993; Droux and Delaloye, 1996; Trumbull et al., 1999; Monzier et al., 1999; Dorendorf, et al., 2000; Richards and Villeneuve, 2001; Matteini et al., 2002). However, although a depletion of MREE may be evidence for amphibole precipitation or the occurrence of amphibole as a residual phase, amphiboles may have been lost from these ash layers during air borne transport from source and this REE pattern may not be an artifact of magna generation. Second, two-ash layers display a more strongly depleted MREE and HREE pattern than the other samples. This pattern may indicate a larger percent of amphibole loss and a greater amount of garnet retention within the source rock, respectively. These two layers also display the same LREE pattern as the other Leg 201 ash layers which may be evidence that these two ash layers have the same source as the other ash samples. Third, not only are the LREE strongly enriched with respect to the HREE, an Eu anomaly is weakly present (Leg 201 ash samples do not show as strong an Eu depletion as many of the samples from the literature), within the REE patterns for most of the ash layers. It is noted in the literature that the presence of a negative Eu anomaly may indicate a depletion of plagioclase within the erupted material. This depletion may occur due to a source rock that contains plagioclase as a residual phase (Taylor and Hallberg, 1977; Rollinson, 1993; Vatin-Perignon, et al., 1996; Richard and Villeneuve, 2001) or plagioclase could be lost (crystallized) from the melt as it ascends (Baker and Francis, 1978; Thorpe and Francis, 1979; de Silva and Francis, 1991). These processes result in a depletion of plagioclase within the final rock which results in a negative Eu anomaly.

The weak presence of a negative Eu anomaly within Leg 201 ash layers indicates a moderate to high concentration of plagioclase within these samples. It is most likely that this abundance of plagioclase is due to the distance of these ash layers from source; the winnowing out of heavier ferromagnesian minerals during air borne transport. Richard and Villeneuve (2001) note that the presence of Eu as Eu^{3+} frequently occurs within fairly oxidized and hydrous arc magmas, resulting in a weak or lacking negative Eu anomaly, as well. A more detailed geochemical investigation of the plagioclase minerals would be necessary to deduce, with any certainty, the true process or processes responsible for the weak negative Eu anomaly displayed by these ash layers.

Ash Layer Correlations

Ash layer correlations between sites were based on lithology, stratigraphic position, and major element geochemistry and have been refined through REE geochemistry. Most ash layers from Sites 1228 and 1229 are the same lithologically, with the primary difference being the percent of volcanic glass or pumice present. Although, half of Site 1229 ash layers correlate with Site 1228 ash layers lithologically (Table 3), some of these ash layers do not correlate stratigraphically.

As previously discussed, most Leg 201 ash layers display the same general major element oxide trends between sites for both glass and whole rock analyses. However, no two-ash layers have identical major element oxide values; therefore no layers are correlated based solely on major element oxides. Due to the lack of definite correlations of ash layers based on lithology, stratigraphic position, and major element oxide concentrations, REE geochemistry was used to refine possible correlations between Leg 201 sites (Fig. 13). Figure 13 displays the stratigraphic correlation of three-ash layer between Sites 1228 and 1229. The REE correlation pair for each these ash layers are also shown in this figure.

Explosive Volcanic Cycles

Many studies have recorded the explosive volcanic cycles of land eruptions through the documentation of ash layers present within deep–sea sediments (Donnelly, 1976; Kennett et al., 1977; Ledbetter and Sparks, 1985; Paterne et al., 1990; Pouclet et al., 1990; Prueher and Rea, 2001). The thickness and number of Type 1 ash layers have

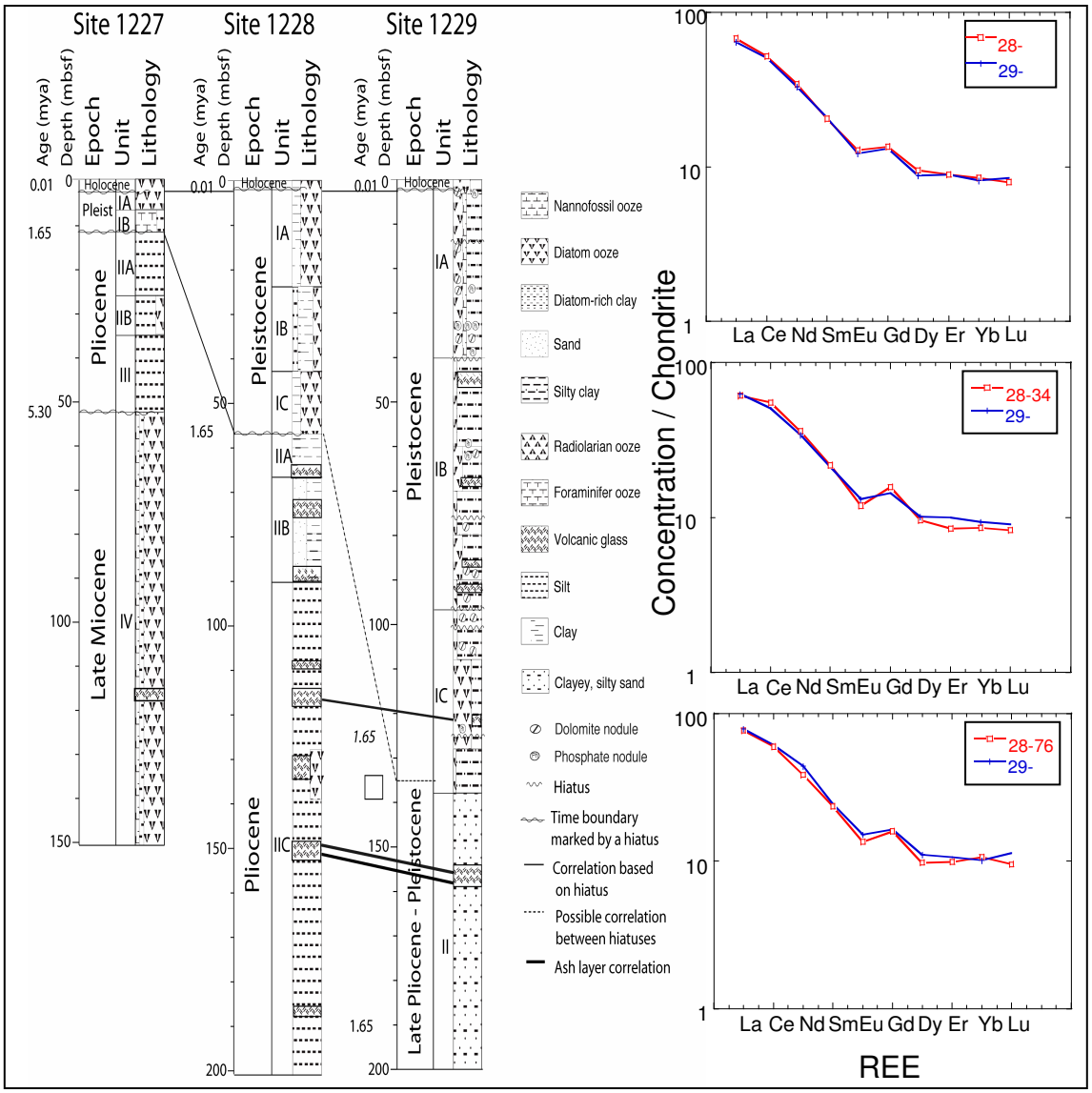

Figure 13: Ash layer correlations. Leg 201 stratigraphic section displaying three ash layer correlations (heavyweight lines) and the corresponding REE pairs (to the right) for each correlation.

been summed for each Leg 201 site in this study, and have been plotted per half million year time increments (Fig. 14, derived from Leg 112 sedimentary rate curves, appendix B) for the purpose of depicting the explosive volcanic cycles for the Central Andes. One limitation in utilizing Leg 112 sedimentation rate curves to depict ash occurrence per half million years from Leg 201 is that the sedimentation rate curves from Leg 112 only extend to 120 mbsf, whereas Type 1 ash is present in Leg 201 Sites 1228 and 1229 cores to 152.74 and 159.55 mbsf, respectively. Additionally, another limitation is that Leg 112 sedimentation rate curves are constructed based upon the first and last occurrence of either diatoms or nannoplankton, which may yield a large error in time (Fig. 14).

This summation does not take accumulations, pods, very thin laminae (< 1 mm), or diagenetically altered layers into account and are therefore minimal estimations at best. Because the sedimentary rate curves from Leg 112 only extend to 120 mbsf while Type 1 is present within Leg 201 Sites 1228 and 1229 cores to a depth of 152.74 and 159.55 mbsf, respectively, Figure 14 is a minimal depiction of explosive activity through time. Additionally, all Leg 201 sites have been affected by sedimentary hiatuses (Fig. 6) and some sections of core display evidence of possible slump deposits and/or turbidites. These features could be a significant factor in the disappearance of ash layers from the marine record. Prevailing wind direction and marine currents are two limiting factors that should also be taken into account when recording volcanic cycles from ash within deep-sea sediments (Pouclet et al., 1990). Since the closest known volcanic source is >400 km from the study region (Fig. 1) it is apparent that wind direction, and to a

smaller extent ocean current, may be responsible for the deposition of ash this far offshore. Figure 4 displays the southwestern trade winds that appear to circulate north northwestward along the Chile coast. These winds appear to follow the Chilean coast up to the Peru coast, where their direction takes on a northwestern path that parallels the Peruvian coast. These winds coupled with the Coriolis force causes a deflection in the Humboldt Current, which circulates northward along the South American western coast to the surrounding area of the equator, thus severing the current from the Peruvian coast (Garcia, 1994). However, other local currents may have had an influence in the deposition of ash into the study region. The air and water circulation patterns illustrated in Figure 4 suggest that volcanic ash erupted into the atmosphere from northern Chile and/or southern Peru would have been transported into the study region by the prevailing trade winds along western South America. However, shifts in wind direction can deposit ash outside the study region and may therefore be a limiting factor when deducing explosive eruption cycles recorded within the marine sediments of Leg 201 cores.

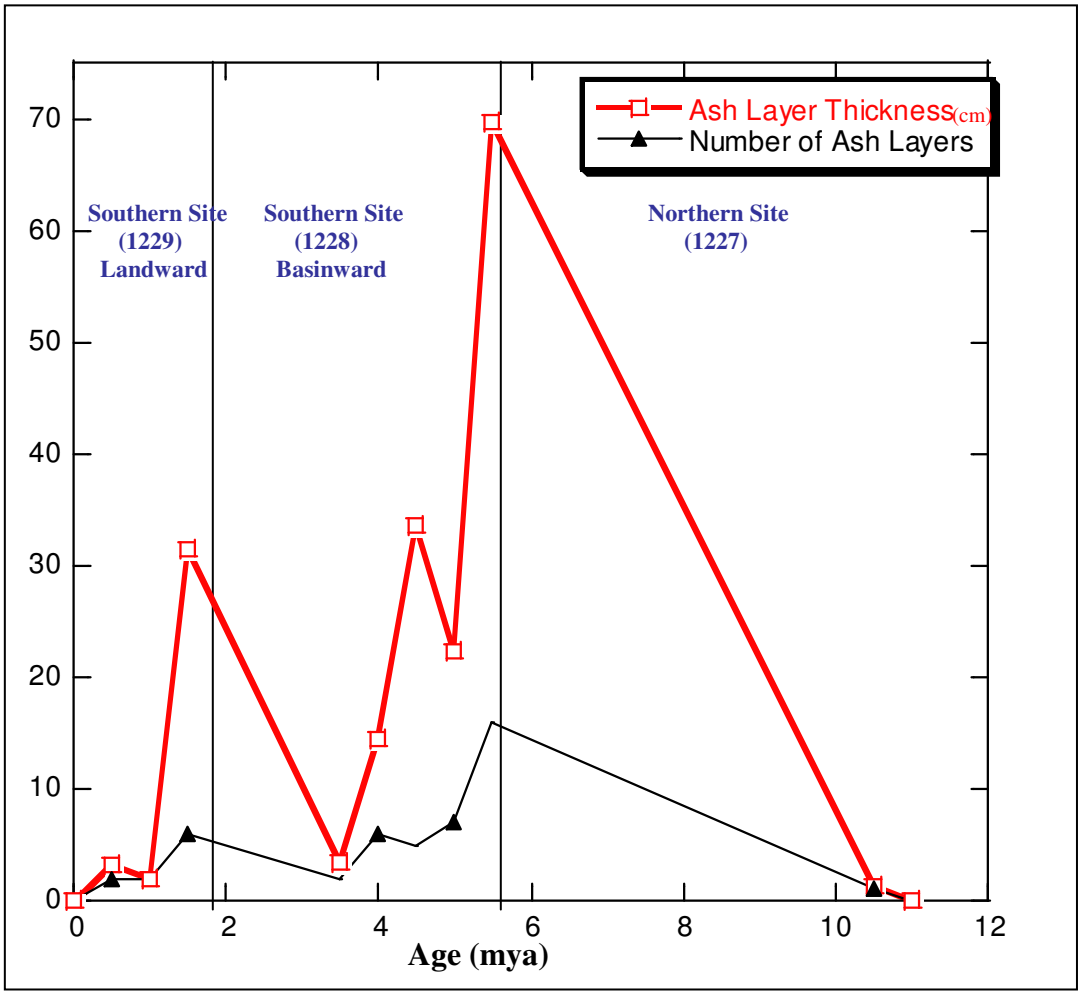

Figure 14: Leg 201 ash layer thickness and number of ash layers plotted per half million year time period.

Figure 14 displays ash layer thickness and the number of ash layers per half million-year time increments. Explosive eruption cycles for the Andean region have been deduced from these data. Our record of volcanic cycles indicates that explosive activity was less intense during the Miocene, in which one ash layer (1.3 cm) was deposited, compared to that of the Pliocene and Pleistocene which experienced most of the explosive volcanic activity in which 52 ash layers (total thickness equal to 208.6 cm) and 14 ash layers (total thickness equal to 122.1 cm) were deposited respectively (Fig. 14). These data are consistent with the previous study of Pouclet et al. (1990); however these data indicate that explosive activity during the Pliocene and Pleistocene was more intense than previously reported. Additionally, the total thickness of Type 1 within all three Leg 201 sites is equal to 332.0 cm, which is approximately 24 times as much Type 1 reported by Pouclet et al. (14 cm, 1990) within the previously occupied sites of Leg 112. However, Pouclet et al. (1990) report three Miocene volcanic phases for the northern and southern sites of Leg 112. In this study only one Miocene ash layer is observed within cores from the northern site (Site 1227, Pouclet et al.'s (1990) Site 684) and no Miocene ashes are observed for Leg 201 southern sites. This discrepancy is due to two factors, first only one Miocene ash layer is present within the northern site studied both here (Hole 1227A) and previously (Site 684); the other two layers reported by Pouclet et al. (1990) were in cores from northern sites that were either not examined during this study or were not reoccupied during Leg 201. Secondly, the southern sites studied by Pouclet et al. (1990) that contained Miocene ash layers were not reoccupied during Leg 201.

DISCUSSION AND CONCLUSIONS

It is well documented that volcanoes of the CVZ of the Central Andes are responsible for producing some of the largest volcanic deposits within the Andean chain (e.g. Noble et al., 1974; Baker and Francis, 1978; Tosdal et al., 1981; Baker, 1981; Lahesen, 1982; Hall and Calle, 1982; Sparks et al., 1985; Francis and de Silva, 1989; de Silva and Francis, 1991; Lindsay et al., 2001). The large ignimbrite deposits of this region are of the most significance for this study since they indicate the likelihood of airborne ash (Baker and Francis, 1978) and large plinian style eruptions, which can produce wide spread air fall ash (Fisher and Schmincke, 1984), such as that deposited off the Peru coast and present within cores from all three Leg 201 sites studied.

From the detailed examination of Leg 201 cores, drilled off the coast of Peru, I have documented one Type 1 ash layer (1.3 cm) for Miocene sediments, 52 Type 1 ash layers (total thickness equal to 208.6 cm) for Pliocene sediments, and 14 Type 1 ash layers (total thickness equal to 122.1 cm) for Pleistocene sediments. The total thickness of Type 1 ash recorded within the marine sediments of this study is 332.0 cm. Even though the thickness of Type 1 calculated for this study is a minimal value it is equal to 47 times that recorded from the previously occupied sites of this region (total thickness 14 cm, summed from table 1 of Pouclet et al., 1990).

The correlation of Leg 201 ash layers with land and other marine studies is based on whole rock and glass major element and whole rock REE geochemistry. As previously

mentioned, these correlations are meant to depict from which volcanic zone/s of the Andes these layers were possibly derived, and are not intended to determine the individual volcano from which these layers were erupted. From the average glass and whole rock geochemistry (Figs. 9 and 11) it is evident that a majority of the intermediate to acidic ash layers was derived from central and/or northern Andean volcanic regions. In addition, REE geochemistry supports the overall derivation of Leg 201 ash layers from the CVZ (Fig. 12).

REE geochemistry has been utilized in this study to refine volcanic ash layer correlations between Leg 201 sites. REE are a useful tool for correlating volcanic ash layers because they are the least soluble trace element, relatively immobile, and in weathered or altered sedimentary rocks their concentrations may become diluted but they usually retain their original fractionation patterns (Cullers et al., 1993; Condie et al., 1995). Figure 13 displays three ash layer correlations between Sites 1228 and 1229. Two of the ash layers are correlated between Pliocene (Site 1228) and Late Pliocene-Pleistocene (Site 1229) sediments. The other ash layer is correlated between Pliocene (Site 1228) and Pleistocene (Site 1229) sediments. The three REE correlation pairs displayed in Figure 13 match very well indicating that each of these three ash layers between sites are the same. This evidence coupled with the qualitative nature of biostratigraphic time boundaries, it can be hypothesized that the time boundaries between Pleistocene and Pliocene sediments in Leg 201 Site 1229 may occur higher in the stratigraphic column

than currently reported. Radiometric age dates would provide a better constraint on these time boundaries.

The explosive cycles of Andean volcanoes are recorded within the marine sediments of all Leg 201 sites studied, as well as within the voluminous deposits of ignimbrites on land. The explosive volcanic cycles documented from Leg 201 sites are consistent with the previous marine study of Pouclet et al. (1990) as well as with those of land based studies. To date, Adams et al., (2001) have documented the largest historic eruption of the Andes, the 1600 AD eruption of Huaynaputina, which deposited ash fall 5 cm thick at a distance of 200 km from the source. However, the occurrence of volcanic ash layers within the marine sediments of Leg 201 sites, with thicknesses varying from < 1 to 13.5 cm at a distance >400 km from any possible source (Fig. 1), is evidence that these ash layers may have been deposited from large explosive eruptions that have not been documented for the Andes.

Table 7 presents the approximate amount of ash, in the form of air-fall or ignimbrite deposits, for land studies and marine regions (the amount of ash for land studies is a sum of calculated volumes per time period from the literature and is presented as a sum of ash layer thickness within cores per time period for the marine regions). In general the land records of Baker and Francis, (1978) and Francis and Hawkesworth (1994) indicate that the greatest volume of eruptions was during the Miocene with a large decrease in activity during the Pliocene. The least amount of volcanic ash was deposited during

Pleistocene and Holocene within the northern area of their study regions. The Type 1 ash record of Leg 201 (Table 3) indicates that only one ash layer was preserved within Miocene age deposits. However, Table 4 records an additional 93 cm of diagenetically altered (Type 4) ash, as well as two very thin laminae within Miocene sediments, eight very thin Type 4 laminae within Pliocene sediments and one very thin Type 4 lamina within Holocene sediments for the northern study region. These data indicate concurrent eruption cycles recorded between the land and marine studies, indicating that the episodicity of eruption material per time period recorded in marine sediments is in accordance with the degree of explosive activity per time period within the northern region, interpreted from land studies. However, the absence of Type 1 or Type 4 volcanic material from the marine record for the Pleistocene may indicate a period of less vigorous volcanism within the Central Andes or a change in prevailing wind or ocean current. However, the lack of volcanic material from this time period could just be an artifact of a less well preserved continuous record for this region. Additionally, the preservation of the thin lamina within Holocene sediments indicates that at least one very explosive eruption took place during this time.

Table 7: Amount of volcanic ash. A comparison of the amount of volcanic ash recorded from land studies, ODP Leg 112, and ODP Leg 201. Approximate quantities of volcanic ash (from ignimbrites and/or air fall) deposited within the central-Andes.

TIME (mya)	AMOUNT OF VOLCANIC ASH		
	Land Studies Volume (km^3)	Leg 112 Ash Layer Thickness (cm)	Leg 201 Ash Layer Thickness (cm)
Miocene	1300	4.8	1.3
Pliocene	650	2.4	194.9
Pleistocene	275	1.2	50

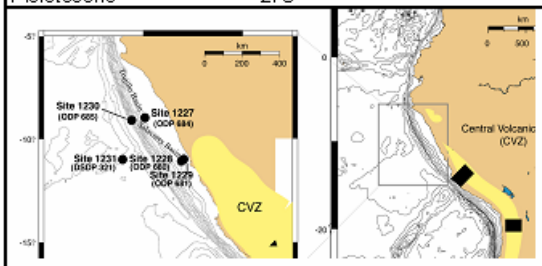

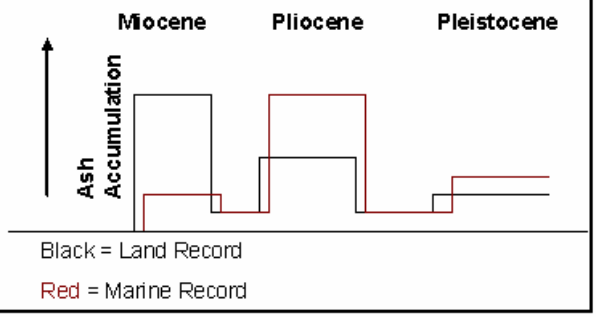

Black = Land Record

Red = Marine Record

A large volume of volcanic material was deposited during the Miocene within the southern study region of Baker and Francis (1978). An even larger amount of material was deposited during the Pliocene, and the least amount of material was erupted during the Pleistocene (Baker and Francis, 1978). The eruption cycles documented on land are mimicked in the marine record indicating concurrent eruption cyclicity. Additionally, three Type 2 ash layers are preserved within Holocene sediments of the southern sites, which may indicate when coupled with the distance from any known source, the possible occurrence of three large magnitude eruptions.

Overall, there appears to be a distinct difference in the volume of volcanic material deposited within the northern and southern study regions of Baker and Francis's (1978), Pouclet et al. (1990), Francis and Hawkesworth (1994), and this study. These variations could be due to an incomplete marine record of Miocene sediments; proximity of volcanic source to Leg 201 study sites and/or it could be directly related to the explosive cycles of the region. A more detailed study of the volcanic ash physiology may aid in determining if these variations directly related to the explosive cycles of the region (e. g. A greater degree of fragmentation of the volcanic ash within the marine sediments of Leg's 201 and 112 would be evidence that the eruptions that produced this material may have been more explosive than some of the land eruptions.

REFERENCES

Adams, N. K., de Silva, S. L., Self, S., Salas, G., Schubring, S., Permenter, J. L., Arbesman, K., 2001. The physical volcanology of the 1600 eruption of Huaynaputina, southern Peru. Bull. Volcanol. 62, 493-518.

Baker, M. C. W., 1981. The nature and distribution of upper Cenozoic ignimbrite centers in the Central Andes. J. Volcanol. Geotherm. Res. 11, 293-315.

Baker, M. C. W., Francis, P. W., 1978. Upper Cenozoic volcanism in the Central Andes – ages and volumes. Earth Planet. Sci. Lett. 41, 175-187.

Condie, K. C., Dengate, J., Cullers, R.L., 1995. Behavior of rare earth elements in a paleoweathering profile on granodiorite in the Front Range, Colorado, USA. Geochimica et Cosmochimica Acta. 59 (2), 279-294.

Cullers, R. L., DiMarco, M. J., Lowe, D. R., Stone, J., 1993. Geochemistry of a silicified, flesic volcaniclastic suite from the early Archaean Panorama Formation, Pilbara Block, Western Australia: an evaluation of depositional and post-depositional processes with special emphasis on the rare-earth elements. Precambrian Res. 60, 99-116.

D'Hondt, S. L., Jorgensen, B. B., Miller, D. J., Aiello, I.W., Bekins, B., et al., 2003. Proc. ODP, Init. Repts., 201 [CD-ROM]. Available from Ocean Drilling Program, Texas A&M University, College Station TX.

D'Orazio, M., Innocenti, F., Manetti, P., Tamponi, M., Tonarini, S., Gonzalez-Ferran, O., Lahesen, A., and Omarini, R., 2003. The Quaternary calc-alkaline volcanism of the Patagonia Andes close to the Chile triple junction: geochemistry and petrogenesis of volcanic rocks from the Cay and Maca volcanoes (~45°S, Chile). J. South Am. Earth Sci. 16, 219-242.

De Silva, S. L., 1989. Geochronology and stratigraphy of the ignimbrites from the $21^{0}30'$ S to $23^{0}30'$ S portion of the Central Andes of northern Chile. J. Volcanol. Geotherm. Res. 37, 93-131.

De Silva, S. L., Francis, P. W., 1989. Correlation of large ignimbrites – Two case studies from the Central Andes of northern Chile. J. Volcanol. Geotherm. Res., 37:133-149.

De Silva, S. L., Francis, P. W., 1991. Volcanoes of the Central Andes. Springer-Verlag New York.

De Silva, S. L., Zielinski, G. A., 1998. Global influence of the AD 1600 eruption of

Huaynaputina, Peru. Nature 393, 455-457.

Donnelly, T. W., 1976. Tertiary explosive volcanic activity in the eastern equatorial Pacific Ocean: Sites 320 and 321, DSDP Leg 34. In: Yeats, R. S., Hart, S. R., et al., (Eds). Init. Repts. DSDP, 34: Washington DC (U.S. Government Printing Office), 605-610.

Dorendorf, F., Churikova, T., Koloskov, A., and Wörner, G., 2000. Late Pleistocene to Holocene activity at Bakening volcano and surrounding monogenetic centers (Kamchatka): volcanic geology and geochemical evolution. J. Volcanol. Geotherm. Res. 104, 131-151.

Dostal, J., Dupuy, C., and Lefevre, C., 1977. Rare earth element distribution in Plio-Quarternary volcanic rocks from southern Peru. Lithos 10 (3), 173-183.

Droux, A., and Delaloye, M., 1996. Petrography and geochemistry of Plio-Quaternary Calc-Alkaline volcanoes of Southwestern Columbia. J. South Am. Earth Sci. 9 (1/2), 27-41.

Fisher, R. V. and Schmincke, H.-U., 1984. Pyroclasic Rocks. Springer-Verlag New York.

Francis, P. W. and Baker, M. C. W., 1978. Sources of two large ignimbrites in the Central Andes: Some Landsat evidence. J. Volcanol. Geotherm. Res. 4, 81-87.

Francis, P. W. and De Silva, S. L., 1989. Application of the Landsat Thematic Mapper to the identification of potentially active volcanoes in the Central Andes. Remote Sens. Environ. 28, 245-255.

Francis, P. W. and Hawkesworth, C. J., 1994. Late Cenozoic rates of magmatic activity in the Central Andes and their relationship to continental crust formation and thickening. J. Geol. Society, London 151, 845-854.

Garcia, N. O., 1994. South American climatology. Quaternary International 21, 7-2.

Gutierrez, A., Gioncada,O., Gonzales, F., Lahesen, A., and Mazzuoli, R., 2005. The Hudson Volcano and surrounding monogenetic centres (Chilean Patagonia): An example of volcanism associated with ridge-trench collision environment. J. Volcanol. Geotherm. Res. 145 (3-4), 207-233.

Hall, M. L. and Calle, J., 1982. Geochronological control for the main tectonic-magmatic events of Ecuador. Earth-Sci. Rev. 18, 215-239.

Hanuš, V. and Vaněk, J., 1978. Morphology of the Andean Wadati-Benioff zone, Andesitic volcanism, and tectonic features of the Nazca plate. Tectonophysics 44, 65-77.

Kennett, J.P., McBirney, A.R., and Thunell R.C., 1977. Episodes of Cenozoic volcanism in the Circum-Pacific region. J. Volcanol. Geotherm. Res. 2, 145-163.

Lackschewitz, K. S. and Wallrabe-Adams, H.-J., 1997. Composition and origin of volcanic ash zones in late Quaternary sediments from the Reykjanes Ridge: evidence for ash fallout and ice-rafting. Mar. Geol. 136, 209-334.

Lahesen, A., 1982. Upper Cenozoic volcanism and tectonism in the Andes of northern Chile. Earth-Sci. Rev. 18, 285-302.

Ledbetter, M. T., 1985. Tephrochronology of marine tephra adjacent to Central America. Geol. Soc. of Am. Bull. 96 (1), 77-82.

Ledbetter, M. T. and Sparks, R. S. J., 1979. Duration of large-magnitude explosive eruptions deduced from graded bedding in deep-sea ash layers. Geology 7, 240-244.

Legros, F., 2001. Tephra stratigraphy of Misti volcano, Peru. J. South Am. Earth Sci. 14, 15-29.

Lindsay, J M., de Silva, S., Trumbull, R., Emmermann, R., Wemmer, K., 2001. La Pacana caldera, N. Chile: a re-evaluation of the stratigraphy and volcanology of one of the world's largest resurgent calderas. J. Volcanol. Geotherm. Res. 106, 145-173.

Matteini, M., Mazzuoli, R., Omarini, R., Cas, R., and Maas, R., 2002. The geochemical variations of the upper Cenozoic volcanism along the Calama-Olacapato-El Toro transversal fault system inn central Andes (~24°S): petrogenetic and geodynamic implications. Tectonophysics 345, 211-227.

Monzier, M., Robin, C., Samaniego, P., Hall, M. L., Cotton, J., Mothes, P., and Arnaud, N., 1999. Sangay volcano, Ecuador: structural development, present activity and petrology. J. Volcanol. Geotherm. Res. 90, 49-79.

Noble, D. C., McKee, E. H., Farrar, E., Petersen, U., 1974. Episodic Cenozoic volcanism and tectonism in the Andes of Peru. Earth Planet. Sci. Lett. 21, 213-220.

Paterne, M., Labeyrie, F., Guichard, F., Mazaud, A., and Maitre, F., 1990. Fluctuations of the Campanian explosive volcanic activity (South Italy) during the past 190,000 years, as determined by marine tephrochronology. Earth Planet. Sci. Lett. 98, 166-174.

Pattan, J. N., Shane, P., and Banakar, V. K., 1999. New occurrence of youngest Toba Tuff in abyssal sediments of the Central Indian Basin. Mar. Geol. 155, 243-248.

Petrinovic I.A., Riller, U., and Brod, J.A., 2005. The Negra Muerta Volcanic Complex, southern Central Andes: geochemical characteristics and magmatic evolution of an episodically active volcanic centre. J. Volcanol. Geotherm. Res. 140, 295-320.

Pouclet, A., Cambray, H., Cadet, J. P., Bourgois, J., and De Wever, P., 1990. Volcanic ash from Leg 112 off Peru. In: Suess, E., von Huene, R., et al., Proceedings of the Ocean Drilling Program, Sci. Results, 112: College Station, TX (Ocean Drilling Program) 465-480.

Prueher, LM., and Rea, D.K., 2001. Tephrochronology of the Kamchatka-Kurile and Aleutian arcs: evidence for volcanic episodicity. J. Volcanol. Geotherm. Res. 106, 67-84.

Richards, J.P., and Villeneuve, M., 2001. The Llullaillaco volcano, northwest Argentine: construction by Pleistocene volcanism and destruction by sector collapse. J. Volcanol. Geotherm. Res. 105, 77-105.

Rollinson, H., 1993. Using geochemical data: evaluation, presentation, interpretation. Essex, England, Pearson Education Limited, Prentic Hall Publishers, 352pp.

Shane, P., 2000. Tephochronology: a New Zealand case study. Earth-Sci. Rev. 49, 223-259.

Siebel, W., Schnurr, W.B.W., Hahne, K., Kraemer, B., Trumbull, R.B., van den Bogaard, P., and Emmermann, R., 2001. Geochemistry and isotope systematics of small- to medium-volume Neogene-Quaternary ignimbrites in the southern central Andes: evidence for derivation from andesitic magma source. Chem. Geol. 171, 213-237.

Sparks, R. S. J., Francis, P. W., Hamer, R. D., Pankhurst, R. J., O'Callaghan, L. O., Thorpe, R. S., and Page, R., 1985. Ignimbrites of the Galan Caldera, NW Argentina. J. Volcanol. Geotherm. Res. 24, 205-248.

Suess, E., von Huene, R., Emeis, K. C., Bourgois, J., Castaneda, J., et al., 1990. Proceedings of the Ocean Drilling Program, Init. Repts. vol. 112: College Station, TX.

Taylor, S.R. and Hallberg, J.A., 1977. Rare-earth elements in the Marda calc-alkaline suite: an Archaen geochemical analogue of Andean-type volcanism. Geochimica et Cosmochimica Acta 41, 1125-1129.

Thorpe, R. S., and Francis, P. W., 1979. Variations in Andean andesite compositions and their pertrogenetic significance. Tectonophysics 57, 53-70.

Thouret, J. C., Davila, J., Rivera, M., Gourgaud, A., Eissen, J.P., Pennec, J.L.L., and Juvigne, E., 1997. The largest explosive eruption (VEI 6) in historical times (1600 AD) in the Central Andes at Huaynaputina, Southern Peru. Earth Planet. Sci. 325, 931-938.

Thouret, J. C., Juvigne, E., Gourgaud, A., Boivin, P., and Davila, J., 2002. Reconstruction of the AD 1600 Huaynaputina eruption based on the correlation of geologic evidence with early Spanish chronicles. J. Volcanol. Geotherm. Res. 115, 529-570.

Tosdal, R. M., Farrar, E., and Clark, A. H., 1981. K-Ar geochronology of the late Cenozoic volcanic rocks of the Cordillera Occidental, southernmost Peru. J. Volcanol. Geotherm. Res. 10, 157-173.

Trumbull, R.B., Wittenbrink, K.H., Emmermann, R., Büsch, W., Gerstenberger, H., and Siebel, W., 1999. Evidence for Late Miocene to Recent contamination of arc andesites by crustal melts in the Chilean Andes (25-26°S) and its geodynamic implications. J. South Am. Earth Sci. 12, 135-155.

Vatin-Perignon, N., Oliver, R.A., Goemans, P., Keller, F., Briqueu, L., and Salas, G.A., 1992. Geodynamic interpretations of plate subduction in the northernmost part of the Central Volcanic Zone from the geochemical evolution and quantification of the crustal contamination of the Nevado Solimana volcano, southern Peru. Tectonophysics 205, 329-355.

Vatin-Perignon, N., Poupeau, G., Oliver, R. A., Lavenu, E., Keller, F., Bellot-Gurlet, L., 1996. Trace and rare-earth element characteristics of acidic tuffs from Southern Peru and Northern Bolivia and a fission-track age for the Sillar of Arequipa. J. South Am. Earth Sci. 9 (5), 91-109.

Yeats, R. S., Hart, S. R., Ade-Hall, J., Bass, M., Benson, W., et al., 1976. Initial Reports of the Deep Sea Drilling Project, volume34, Washington DC (U.S. Government Printing Office) 705 – 712 pp.

APPENDIX A

Table 8
Leg 201 ash sample location. Locations within cores and depth (meters below sea floor) of th
centimeter.

SAMPLE #	Core-Section, Interval (cm)	MBSF	SAMPLE #	Core-Section, Interval (cm)	MBSF
Site 1227					
*27A-1	*13-2, 146 - 147.6	115.07			
Site 1228			**Site 1228 Cont.**		
28A-4	2-6, 121.2 - 121.7	64.24	*28A-59	*16-4, 27 - 40.5	133.17
28A-5	8-2, 83.5 - 84	66.04	*28A-60**	*16-4, 40.5 - 42.5**	133.31
*28A-6	*8-3, 114 - 117	72.09	*28A-64	*18-1, 48 - 56.5	147.88
*28A-10	*9-1, 69.8 - 72	72.12	*28A-65	*18-1, 62 - 67	148.02
28A-11	9-1, 72 - 73	72.15	*28A-67	*18-2, 5.8 - 9.5	148.96
*28A-12	*9-1, 74.5 - 77	72.22	*28A-70	*18-2, 50.5 - 57.5	149.41
28A-13	9-1, 81.5 - 83	72.37	*28A-71	*18-2, 79.7 - 82.9	149.70
*28A-14	*9-1, 97 - 101.6	72.61	*28A-73	*18-2, 88 - 90	149.78
*28A-16	*9-1, 121.4 - 124	91.73	*28A-75	*18-2, 112 - 115	150.02
*28A-19	*11-2, 32.5 - 37.5	91.73	*28A-76	*18-3, 95.5 - 97	151.36
*28A-20	*11-2, 50.2 - 52.3	91.90	*28A-77	*18-4, 0 - 3	151.95
28A-21	11-2, 52.3 - 55	91.93	*28A-80	*18-4, 38 - 42	152.28
*28A-22	*11-2, 55 - 56.6	91.95	*28A-81	*18-4, 49 - 55	152.35
*28A-23	*11-2, 59 - 60.6	91.99	*28A-82	*18-4, 83.5 - 88	152.74
*28A-25	*14-2, 8.1 - 11.7	111.98			
28A-26**	14-2, 116.5 - 117.5**	113.06	**Site 1229**		
28A-27	14-2, 129.3 - 130.2	123.19	29A-a	1-2, 99.6 - 99.9	2.50
28A-29**	14-2, 144 - 149**	113.34	*29A-1**	*3-3, 50 - 50.5**	17.90
*28A-30	*14-5, 52.8 - 59	116.93	*29A-2	*5-5, 126 - 129	40.66
28A-31	14-5, 96.5 - 100	117.37	*29A-3**	*6-3, 18.7 - 20 **	43.09
*28A-32	*14-5, 117.4 - 121.6	117.57	*29A-4	*8-3, 107 - 109	69.97
28A-33	14-5, 132.5 - 133.5	117.72	*29A-6	*10-5, 37 - 44	85.77
*28A-34**	*14-6, 17.3 - 23**	118.07	29A-b**	11-3, 2- 6.5**	91.92
28A-35**	14-6, 23.5 - 26.5**	118.14	*29A-7	*11-3, 6.5 - 9.2	91.97
*28A-37	*16-1, 36.5 - 43	128.77	29A-c	11-3, 10.2	92.00
*28A-38	*16-1, 44 - 48	128.84	29A-d**	11-3, 39.3 - 39.6**	92.29
*28A-39	*16-1, 60 - 64	129.00	29A-e**	11-3, 49.5 - 50.5**	92.80
*28A-40	*16-1, 64.5 - 67	129.05	29A-f**	14-1, 88.3 - 88.5**	118.28
28A-41	16-1, 92 - 96	129.32	29A-g	14-4, 18.5 - 23	122.08
28A-42	16-1, 110.8 - 112	129.51	29A-h**	14-4, 139.2**	123.29
28A-43	16-1, 114 - 117.5	129.54	29A-i**	14-5, 32.5 - 43.5	123.73
*28A-45	*16-1, 118.5 - 123	129.59	*29A-8**	*14-5, 50 - 56**	123.90
28A-46	16-1, 132 - 133	129.72	*29A-9	*18-1, 0 - 3	155.40
*28A-47	*16-2, 12.5 - 16	130.03	29A-j**	18-1, 25 - 74**	155.65
*28A-49	*16-2, 27.5 - 34	130.18	*29A-11	*18-2, 115 - 115.5	158.07
*28A-50	*16-2, 118.5 - 124	131.09	*29A-12	*18-2, 117.2 - 117.4	158.07
*28A-54	*16-3, 96 - 98.5	132.35	*29A-13	*18-2, 117.4 - 127	158.87
*28A-56	*16-3, 110.5 - 114	132.51	*29A-14**	*18-3, 48 - 56**	159.88
*28A-57	*16-3, 118 - 121.5	132.58	*29A-16**	*18-3, 114.5 - 122**	159.95

*= Whole rock geochemical analysis has been attained for these samples to verify purity of these ash layers.
** = Layer is borderline (>= 10-15 % biogenic or dolomite). Whole rock geochemical analysis has been attained for some of the lower end borderline layers (these samples have a number versus a letter in the sample number column).

APPENDIX B

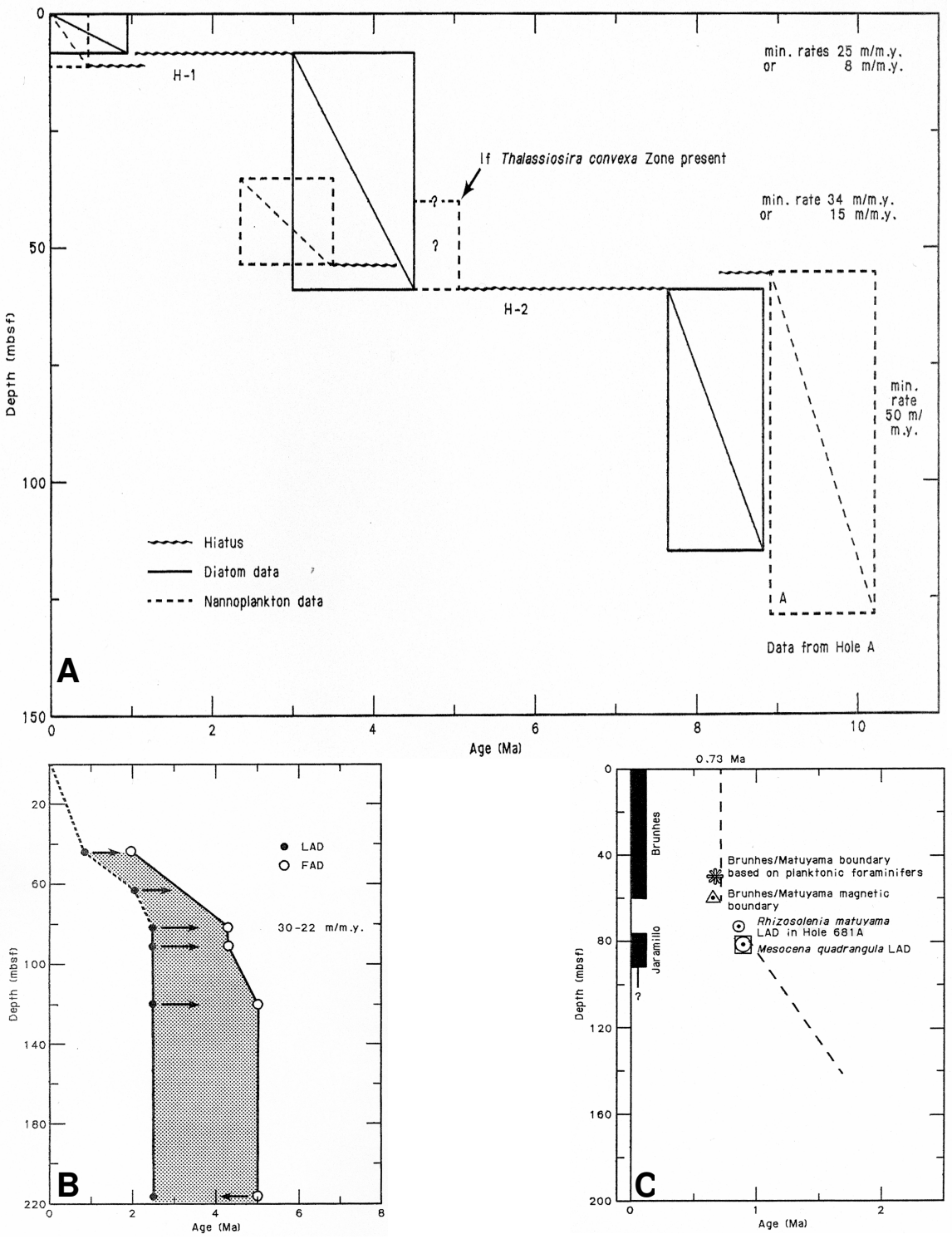

Figure 15: Leg 112 sedimentation rate curves. Curves are based on first and last occurrences of fossil assemblages. A) This set of curves are from Site 684 and were used during this study to determine ash occurrences between 9.5-10 mya. B) This set of curves is from Site 280 and were used in this study to determine ash occurrences between 2-5 mya. C) This set of curves is from Site 681 and were used in this study to determine ash occurrences between 1-2 mya. (From Suess, von Huene, et al., 1990).

VITA

Shirley Dawn Hart

Employment Address:
Core Laboratories
Integrated Reservoir Solutions Division
6316 Windfern
Houston, TX 77040

Employment Phone Number:
(713) 328-2673
Direct Dial: (713) 328-2671

Education:
Texas A&M University
Bachelor of Science, Geology
August 2002

Texas A&M University
Master of Science, Geology
December 2006